

ABSTRACT

Title of Document: PROGNOSTICS OF SOLDER JOINT
RELIABILITY UNDER VIBRATION
LOADING USING PHYSICS OF FAILURE
APPROACH

Jie Gu, Doctor of Philosophy (Ph.D.), 2009

Directed By: Chair Professor and Director, Michael G. Pecht,
Department of Mechanical Engineering

Physics-of-failure (PoF) is an approach that utilizes knowledge of a product's life cycle loading and failure mechanisms to perform reliability modeling, design, and assessment. Prognostics is the process of predicting the future reliability of a system by assessing the extent of deviation or degradation of a product from its expected normal operating states. When prognostics is combined with physics-of-failure models, it is possible to make continuously updated reliability predictions based on the monitoring of the actual environmental and operational conditions of each individual product.

A literature review showed that the research on prognostics of solder joint reliability under vibration loading is very limited. However, personal portable electronic products are no longer used exclusively in a benign office environment. For example, any electronic component (throttles, brakes, or steering) in an automobile should be able to survive in a vibration environment.

In this thesis, a methodology was developed for monitoring, recording, and analyzing the life-cycle vibration loads for remaining-life prognostics of solder joints. The responses of printed circuit boards (PCB) to vibration loading were monitored using strain gauges and accelerometers, and they were further transferred to solder strain and stress for damage assessment using a failure fatigue model. Damage estimates were accumulated using Miner's rule after every mission and then used to predict the life consumed and the remaining life. The results were verified by experimentally measuring component lives through real-time daisy-chain resistance measurements.

This thesis also presents an uncertainty assessment method for remaining life prognostics of solder joints under vibration loading. Basic steps include uncertainty source categorization, sensitivity analysis, uncertainty propagation, and remaining life probability calculation. Five types of uncertainties were categorized, including measurement uncertainty, parameter uncertainty, model uncertainty, failure criteria uncertainty, and future usage uncertainty. Sensitivity analysis was then used to identify the dominant input variables that influence model output. After that, a Monte Carlo simulation was used for uncertainty propagation and to provide a distribution of accumulated damage. From the accumulated damage distributions, the remaining life was then able to be predicted with confidence intervals. The results showed that the experimentally measured failure time was within the bounds of the uncertainty analysis prediction.

PROGNOSTICS OF SOLDER JOINT RELIABILITY UNDER VIBRATION
LOADING USING PHYSICS OF FAILURE APPROACH

By

Jie Gu

Dissertation submitted to the Faculty of the Graduate School of the
University of Maryland, College Park, in partial fulfillment
of the requirements for the degree of
Doctor of Philosophy
2009

Advisory Committee:
Professor Michael G. Pecht, Chair
Professor Donald Barker
Professor Bilal Ayyub
Associate Professor Peter Sandborn
Associate Professor F. Patrick McCluskey

© Copyright by
Jie Gu
2009

Dedication

This thesis is dedicated to my family and my parents, who taught me never to give up.

Acknowledgements

With a deep sense of gratitude, I wish to express my sincere thanks to my advisor Prof. Michael Pecht for allowing me to work on this interesting topic and continuously challenging me to set my benchmark higher.

I would also like to thank Prof. Barker, Prof. Ayyub, Prof. Sandborn, and Prof. McCluskey for serving on my dissertation committee and providing valuable suggestions from time to time. I also appreciate Prof. Dasgupta's guidance on my dissertation work from time to time.

I am thankful to the CALCE staff, including Dr. Azarian, Dr. Das, Dr. Osterman, Sony Mathew, Anshul Shrivastava, Bhanu Sood, Joan Lee, David Eisner and Cindy Wang, for their kindness and support.

I wish to express very special thanks to all of my friends at CALCE, including Sachin Kumar, Vasilis Sotiris, Hyunseok Oh, Lei Nie, Shunfeng Cheng, Weiqiang Wang, Xiaofei He, Jun Dai, Sunong Zhang, Nishad Patil, Daeil Kwon, Mark Zimmerman, Eli Dolev, Khuu, Vinh, Qingguo Fan, Robert Riddle, Abraham Tomy, Adam Montjoy, Navid Charoosheh, Rubyca Jaai, Rui Wu, Yong Wang, Hongbo Bi, who have been so helpful to me during my graduate experience. I also wish to thank all of my former friends and colleagues at CALCE, including Dr. Vichare, Dr. Qi, Yuxun Zhou, Brian Tuchband, Dr. Rogers, Gustavo Plaza, Reza Keimasi, Yan Liu, Yuliang Deng, Bo Song, Shirsho Sengupta, and Ping Zhao for their support.

Finally, I would like to thank my wife (Liping Ding) and my parents for their constant encouragement and support.

Table of Contents

CHAPTER 1: INTRODUCTION	1
1.1 MOTIVATION AND OBJECTIVE	2
1.2 OVERVIEW OF THESIS.....	3
CHAPTER 2: LITERATURE REVIEW	4
2.1 RELIABILITY ASSESSMENT OF SOLDER JOINT UNDER VIBRATION LOADING.....	4
2.2 PoF IMPLEMENTATION INTO PROGNOSTICS OF ELECTRONICS.....	7
2.3 PROGNOSTICS IMPLEMENTATION PROCEDURE.....	14
2.4 UNCERTAINTY STUDIES ON PROGNOSTICS.....	19
2.5 SUMMAY	20
CHAPTER 3: IN-SITU VIBRATION LOADS MONITORING FOR ELECTRONIC PRODUCTS.....	21
3.1 VIBRATION LOADING MONITORING FOR WASHING MACHINE	21
3.2 VIBRATION LOADING MONITORING FOR NOTEBOOK COMPUTER.....	23
3.3 SUMMARY	26
CHAPTER 4: PROGNOSTICS AND HEALTH MANAGEMENT OF ELECTRONICS UNDER VIBRATION LOADING	27
4.1 PROGNOSTICS APPROACH FOR ELECTRONICS UNDER VIBRATION LOADING ..	27
4.1.1 <i>Characterization of the test board</i>	28
4.1.2 <i>Transfer function from PCB strain/acceleration to solder strain</i>	30
4.2 EQUIPMENT SETUP AND PROCESS	43
4.2.1 <i>Vibration shaker setup</i>	43
4.2.2 <i>Sensor location and data acquisition setup</i>	45
4.2.3 <i>Resistance measurement</i>	51
4.2.4 <i>Strain/acceleration transfer function verification</i>	51
4.2.5 <i>Damage calculation and remaining life prediction</i>	52
4.3 SUMMARY	57
CHAPTER 5: UNCERTAINTY ASSESSMENT OF PROGNOSTICS OF SOLDER JOINTS RELIABILITY.....	59
5.1 UNCERTAINTY ASSESSMENT APPROACH.....	59
5.2 UNCERTAINTY SOURCE CATEGORIZATION	61
5.2.1 <i>Measurement uncertainty</i>	62
5.2.2 <i>Parameter uncertainty</i>	63
5.2.3 <i>Model uncertainty</i>	64
5.2.4 <i>Failure criteria uncertainty</i>	67
5.2.5 <i>Future usage uncertainty</i>	67
5.3 SENSITIVITY ANALYSIS	68
5.4 UNCERTAINTY PROPAGATION	72

5.5	PREDICTION CONSIDERING FAILURE CRITERIA UNCERTAINTY	81
5.6	PREDICTION CONSIDERING FUTURE USAGE UNCERTAINTY	83
5.7	SUMMARY	88
CHAPTER 6: CONTRIBUTIONS AND FUTURE WORK.....		90
APPENDIX A: COMBINED LOADING CALCULATION.....		92
APPENDIX B: CYCLE COUNTING		95
APPENDIX C: MONTE CARLO SIMULATION		100
REFERENCES		102

List of Figures

Figure 1. PoF-based prognostics approach	14
Figure 2. Load feature extraction	17
Figure 3. Vibration monitoring for washing machine – sensor locations	22
Figure 4. Vibration monitoring for washing machine – G level	22
Figure 5. Sensor location for vibration monitoring of notebook computer	23
Figure 6. Vibration levels for one day transportation	24
Figure 7. Vibration levels for one transportation route	24
Figure 8. Vibration variation for a single user during different days	25
Figure 9. One day’s vibration variation for ten computers with different users	26
Figure 10. The prognostics approach for electronics under vibration loading	28
Figure 11. Test board for demonstration of prognostics under vibration	29
Figure 12. Local FEA analysis for strain transfer function	31
Figure 13. Strain relationship between PCB strain and solder strain	31
Figure 14. 2D analytical model for strain transfer function	32
Figure 15. 3D analytical model of full grid array for strain transfer function	34
Figure 16. Interconnect factor parameter estimation	36
Figure 17. 3D analytical model of peripheral array for strain transfer function	38
Figure 18. Modal analysis for PCB	40
Figure 19. FFT analysis for the initial vibration test	40
Figure 20. Strain relationship between boards with and without components	42
Figure 21. Test board mounted on the vibration shaker	44
Figure 22. Random vibration loading input profile	44
Figure 23. Strain gauge locations on the PCB	46
Figure 24. Combined trigger signal recording	48
Figure 25. Initial tests for vibration tests	49
Figure 26. Vibration acceleration histogram comparison	50
Figure 27. Sensor location illustration	52
Figure 28. Accumulated damage for component BGA 352-1	54
Figure 29. Remaining life prediction for component BGA352-1	55
Figure 30. Comparison of remaining life prediction using different sensors	57
Figure 31. Uncertainty source in PoF based prognostics procedure	60
Figure 32. Uncertainty assessment approach	61
Figure 33. S-N curve	64
Figure 34. S-N curve with different failure probabilities	66
Figure 35. Confidence interval for S-N curve	66
Figure 36. Uncertainty range	70
Figure 37. Damage uncertainty range for the first hour	71
Figure 38. Uncertainty propagation	73
Figure 39. Uncertainty analysis procedure for prognostics	75
Figure 40. Input parameters for Monte Carlo simulation	77
Figure 41. Accumulated damage distribution for one hour	78
Figure 42. Uncertainty propagation with damage accumulation	79
Figure 43. Damage accumulation with time at different failure probabilities	79
Figure 44. Remaining life prediction at different failure probabilities	80

Figure 45. Conditional reliability estimation	81
Figure 46. Remaining life prediction considering failure criteria uncertainty.....	83
Figure 47. Future loading categorizations from accumulated damage	84
Figure 48. Remaining life prediction considering future usage uncertainty.....	86
Figure 49. Updated remaining life prediction considering future usage uncertainty .	88
Figure 50. Time triggered recording.....	92
Figure 51. Signal triggered recording.....	93
Figure 52. Cycle identification	96
Figure 53. Rainflow cycle counting.....	99

List of Tables

Table 1. Life cycle loads.....	15
Table 2. Failure mechanisms, relevant loads, and models for electronics.....	18
Table 3. Natural frequency of the test board.....	29
Table 4. PCB strain and solder strain relationship for BGA components	37
Table 5. Vibration step stress test matrix.....	44
Table 6. Signal recording method comparison for lab test data	48
Table 7. Signal recording method comparison for road test data	48
Table 8. Local PCB strain / Middle PCB strain.....	52
Table 9. Middle PCB strain / Middle PCB acceleration ($\mu\epsilon/G$)	52
Table 10. Remaining life prediction using accelerometer	56
Table 11. Failure mechanisms, failure models, and loads	61
Table 12. Sensitivity analysis for uncertainty parameters	69
Table 13. Damage uncertainty range for the first hour.....	72
Table 14. Failure criteria uncertainty categorization	82
Table 15. Remaining life prediction considering failure criteria uncertainty	83
Table 16. Future usage loading level categorization	85
Table 17. Remaining life prediction considering future usage uncertainty	86

Chapter 1: Introduction

Reliability is the ability of a product or system to perform as intended (i.e., without failure and within specified performance limits) for a specified time in its life-cycle environment. Commonly used electronics reliability prediction methods (e.g., Mil-HDBK-217, 217-PLUS, PRISM, Telcordia, FIDES) based on handbook methods have been discredited as they have often provided erroneous life predictions [1][2][3][4][5]. This weakness has led the U.S. military to abandon their electronics reliability prediction methods. The use of stress and damage models permits a far superior accounting of product reliability and the physics of failure; however, sufficient knowledge of the actual operating and environmental application conditions of the product are still required.

Prognostics is the process of predicting the future reliability of a system by assessing the extent of deviation or degradation of a product from its expected normal operating states [6]. By combining prognostics with the physics of failure (PoF) it is possible to make continuously updated predictions based on the monitoring of the actual environmental and operational conditions of each individual product. PoF-based prognostics integrates sensor data with models that enable in-situ reliability assessment.

1.1 Motivation and objective

Assessing the extent of deviation or degradation from an expected normal operating condition (i.e., health) for electronics provides data that can be used to meet several critical goals: (1) advance warning of failures; (2) minimizing unscheduled maintenance, extending maintenance cycles, and maintaining effectiveness through timely repair actions; (3) reducing the life-cycle cost of equipment by decreasing inspection costs, downtime, and inventory; and (4) improving qualification and assisting in the design and logistical support of fielded and future systems [6].

The importance of prognostics and health management has been explicitly stated in the U.S. Department of Defense 5000.2 policy document on defense acquisition, which states that “program managers shall optimize operational readiness through affordable, integrated, embedded diagnostics and prognostics, embedded training and testing, serialized item management, automatic identification technology, and iterative technology refreshment” [7]. Thus, a prognostics capability has become a requirement for any system sold to the Department of Defense.

As the literature review in Chapter 2 shows, while some research has been conducted on reliability estimation of solder joints under vibration loading, research on the prognostics of solder joint reliability under vibration loading has been very limited. However, personal portable electronic products are no longer exclusively used in a benign office environment. For example, any electronic component (throttles, brakes, or steering) in an automobile should be able to survive in a vibration environment.

Therefore, the objective of this thesis is to develop a PoF based prognostic approach for remaining life prediction of solder joints under vibration loading, and develop the uncertainty assessment approach during the prognostics process.

1.2 Overview of thesis

The structure of this thesis is as follows: Chapter 2 provides a literature review of research on assessment of the reliability of solder joints under vibration loading and PoF implementation in prognostics. Chapter 3 presents two case studies on in-situ vibration monitoring of electronic products. Chapter 4 develops a PoF-based prognostics methodology for solder joint reliability under vibration loading. Chapter 5 describes the uncertainty analysis approach to the prognostics of solder joint reliability under vibration loading. Chapter 6 lists the contributions of this thesis and discusses possible future work.

Chapter 2: Literature Review

2.1 Reliability assessment of solder joint under vibration loading

The literature review for this part is categorized into two sections: (1) experimental work, and (2) modeling and simulation work.

(1) Experimental work:

Lau [8] studied solder joint reliability under shock and vibration. He conducted in-plane and out-of-plane random vibration testing. He experimentally studied the solder joint reliability of five different surface mount connectors. The natural frequencies, excitation frequencies, excitation magnitude, velocity, and acceleration of the solder bumped flip chip vibration system have been systematically and carefully determined in this work.

Lee et al. [9] developed a fatigue-testing system to study the integrity of electronic packaging subjected to mechanical vibration. An experimental method was developed to measure the changes in electrical resistance in the lead, which is used to indicate a fatigue. A relationship between the loading force and the fatigue life of the high-cycle region was discussed for the lead of spider gull-wing type surface mount components. The onset of failure was measured by monitoring changes in resistance of daisy chained circuits.

Zhou et al. [10][11] studied the vibration durability of SnAgCu (SAC) solders and SnPb solder using selected surface mount technology (SMT) interconnects. A time domain approach was adopted for this study. The test assembly consists of daisy-chained components to facilitate real-time failure monitoring. In general, the SAC solders were found to have lower fatigue durability than the SnPb solder under the vibration excitation levels applied in this study.

More experimental work on solder joint reliability under vibration can be found from research of Basaran et al. [12], Yang, et al. [13], Wong, et al. [14][15], and Qi et al. [16].

(2) Modeling and simulation work:

The stress-life approach, also called Basquin's damage model [17], relates the stress amplitude to cycles-to-failure in a power law form with the help of two temperature-dependent material constants (fatigue strength coefficient and fatigue damage exponent) that are usually determined empirically. The Equation is listed as follows:

$$N\sigma^b = C \tag{2-1}$$

where C is the fatigue strength coefficient, and b is the fatigue damage exponent.

Steinberg [18] provided an empirical approach that was based on the critical printed circuit board (PCB) displacement. Steinberg assumed the PWB was simply

supported along all four edges. Thus the maximum PWB displacement and maximum PWB curvature occurs at the center of the PWB, and this is where Steinberg assumed the most fatigue damage occurred. For components mounted at other positions on the PWB, a position factor is used to scale the damage. The model also accounts for different package styles. The equation is shown as follows:

$$Z_0 = \frac{0.00022B}{chr\sqrt{L}} \quad (2-2)$$

where Z is the maximum or critical PCB displacement; B is the length of the PWB edge parallel to component; L is the length of electronic component; h is height or thickness of PWB; r is the relative position factor for component on the printed wiring board; and c is constant for different types of electronic components.

Sidharth et al. [19] provided an analytical approach and addressed the determination of the out-of-plane displacements of the corner leads of peripheral leaded components when the local peripheral leaded component/board assembly is subjected to bending moments in two directions (along x and y directions).

Pitarresi et al. [20] used the simple plate vibration models, various material/geometric property smearing approaches, as well as detailed finite element modeling. Smearing techniques derive their name from the fact that the material and geometric properties are smeared in an effort to reduce the complexity of the model. This saved computation time.

More modeling and simulation work on solder joint reliability under vibration can be found in the research of Suhir [21], Barker et al. [22], Engel [23], Singal et al. [24], Darbha et al. [25], Roberts et al. [26], Jih et al. [27], Wong et al. [28], Li [29], and Perkins [30].

2.2 *PoF implementation into prognostics of electronics*

Various studies have been conducted to implement PoF-based prognostics for electronics products. The life cycle loads are monitored, and used in conjunction with PoF-based damage models to assess the degradation due to cumulative load exposures. In the PoF-based prognostics approach, the extent and rate of product degradation depends upon the magnitude and duration of exposure to loads (usage rate, frequency, and severity). A summary of these studies is provided here.

In the study of Ramakrishnan et al., [31] and Mishra et al., [32], the test vehicle consisted of an electronic component board assembly placed under the hood of an automobile and subjected to normal driving conditions in the Washington, D.C., area. The test board incorporated eight surface-mount leadless inductors soldered onto an FR-4 substrate using eutectic tin-lead solder. Solder joint fatigue was identified as the dominant failure mechanism. Temperature and vibrations were measured in situ on the board in the application environment. Using the monitored environmental data, stress and damage models were developed and used to estimate consumed life.

Shetty et al. [33] applied the prognostics methodology for conducting a prognostic remaining-life assessment of the End Effector Electronics Unit (EEEU) inside the robotic arm of the space shuttle remote manipulator system (SMRS). A life-cycle loading profile for thermal and vibration loads was developed for the EEEU boards. Damage assessment was conducted using physics-based mechanical and thermo-mechanical damage models. A prognostic estimate using a combination of damage models, inspection, and accelerated testing showed that there was little degradation in the electronics and they could be expected to last another twenty years.

Mathew et al. [34][35] applied the prognostics methodology to conduct a prognostic remaining-life assessment of circuit cards inside a space shuttle solid rocket booster (SRB). Vibration time history recorded on the SRB from the pre-launch stage to splashdown was used in conjunction with physics-based models to assess damage. Using the entire life-cycle loading profile of the SRBs, the remaining life of the components and structures on the circuit cards was predicted. It was determined that an electrical failure was not expected within another forty missions.

Simons et al. [36] performed a PoF-based prognostics methodology for failure of a gull-wing lead power supply chip on a DC/DC voltage converter PCB assembly. First, three-dimensional finite element analyses (FEA) were performed to determine strains in the solder joint due to thermal or mechanical cycling of the component. The strains could be due to lead bending resulting from the thermal mismatch of the board and chip and those resulting from local thermal mismatch between the lead and the solder, as well as between the board and the solder. Then the strains were used to set

boundary conditions for an explicit model that could simulate initiation and growth of cracks in the microstructure of the solder joint. Finally, based on the growth rate of the cracks in the solder joint, estimates were made of the cycles to failure for the electronic component.

Nasser et al. [37] applied prognostics methodology to predict failure of the power supply. They subdivided the power supply into component elements based on specific material characteristics. Predicted degradation within any single or combination of component elements could be rolled up into an overall reliability prediction for the entire power supply system. Their prognostics technique consisted of five steps: (1) acquiring the temperature profile using sensors; (2) conducting FEA to perform stress analysis; (3) conducting fatigue prediction of each solder joint; (4) predicting the probability of failure of the power supply system.

Searls et al. [38] undertook in situ environment loading, such as temperature measurements, in both notebook and desktop computers used in different parts of the world. In terms of the commercial applications of this approach, IBM has installed temperature sensors on hard drives (Drive-TIP) [39] to mitigate risks due to severe temperature conditions, such as thermal tilt of the disk stack and actuator arm, off-track writing, data corruptions on adjacent cylinders, and outgassing of lubricants on the spindle motor.

Vichare et al. [40][41] also conducted in situ health monitoring of notebook computers. The authors monitored and statistically analyzed the temperatures inside a notebook computer, including those experienced during usage, storage, and

transportation, and discussed the need to collect such data both to improve the thermal design of the product and to monitor prognostic health. After the data was collected, it could be used to estimate the distributions of the load parameters. The usage history was used for damage accumulation and remaining life prediction.

In 2001, the European Union funded a four-year project, “Environmental Life-Cycle Information Management and Acquisition” (ELIMA), which aimed to develop ways to manage the life cycles of products [42][43]. The objective of this work was to predict the remaining life time of parts removed from products, based on dynamic data, such as operation time, temperature, and power consumption. As a case study, the member companies monitored the application conditions of a game console and a household refrigerator. The work concluded that in general, it was essential to consider the environments associated with all life intervals of the equipment. These included not only the operational and maintenance environments, but also the pre-operational environments, when stresses maybe imposed on the parts during manufacturing, assembly, inspection, testing, shipping, and installation. Such stresses are often overlooked, but can have a significant impact on the eventual reliability of equipment.

Tuchband et al. [44] presented the use of prognostics for a military line replaceable units (LRU) based on their life cycle loads. The study was part of an effort funded by the Office of Secretary of Defense to develop an interactive supply chain system for the U.S. military. The objective was to integrate prognostics, wireless communication, and databases through a web portal to enable cost-effective

maintenance and replacement of electronics. The study showed that prognostics-based maintenance scheduling could be implemented into military electronic systems. The approach involves an integration of embedded sensors on the LRU, wireless communication for data transmission, a PoF-based algorithm for data simplification and damage estimation, and a method for uploading this information to the Internet. Finally, the use of prognostics for electronic military systems enabled failure avoidance, high availability, and reduction of life cycle costs.

Canary devices mounted on the actual product have been used to provide advance warning of failure due to specific wearout failure mechanisms. The word “canary” is derived from one of coal mining’s earliest systems for warning of the presence of hazardous gas using the canary bird. Because the canary is more sensitive to hazardous gases than humans, the death or sickening of the canary was an indication to the miners to get out of the shaft. The same approach, using canaries, has been employed in prognostics. Canary devices were integrated into a specific component, device, or system design and incorporated failure mechanisms that occur first in the embedded device. These embedded canary devices (also called prognostics cell) were non-critical elements of the overall design providing early incipient failure warnings before actual system or component failure [45].

Mishra et al. [46] studied the applicability of semiconductor level health monitors by using pre-calibrated cells (circuits) located on the same chip with the actual circuitry. The prognostics cell approach was commercialized by Ridgetop Group to provide an early-warning sentinel for upcoming device failures [47]. The

prognostic cells were available for 0.35, 0.25, and 0.18 micron CMOS processes. The time to failure of these prognostic cells could be pre-calibrated with respect to the time to failure of the actual product. The stresses that contributed to degradation of the circuit included voltage, current, temperature, humidity, and radiation. Since the operational stresses were the same, the damage rate was expected to be the same for both the circuits. However, the prognostic cell was designed to fail earlier due to increased stress on the cell structure by means of scaling. For example, scaling could be achieved by controlled increase of the current density inside the cells. With the same amount of current passing through both circuits, if the cross-sectional area of the current-carrying paths in the cells was decreased, a higher current density was achieved. Not only structure could be scaled, the loading also could be scaled. Further control in current density could be achieved by increasing the voltage level applied to the cells. Higher current density led to higher internal heating, causing greater stress on the cells. When a current of higher density passed through the cells, they were expected to fail faster than the actual circuit [45]. Currently, prognostic cells are available for semiconductor failure mechanisms such as electrostatic discharge (ESD), hot carrier, metal migration, dielectric breakdown, and radiation effects.

The extension of this approach to board-level failures was proposed by Anderson et al. [48], who created canary components (located on the same printed circuit board) that include the same mechanisms that lead to failure in actual components. Anderson et al. identified two prospective failure mechanisms: (1) low cycle fatigue of solder joints, assessed by monitoring solder joints on and within the canary package; and (2) corrosion monitoring using circuits that will be susceptible to

corrosion. The environmental degradation of these canaries was assessed using accelerated testing, and degradation levels were calibrated and correlated to actual failure levels of the main system.

Goodman et al. [49] used a prognostic cell to monitor time-dependent dielectric breakdown (TDDB) of the metal-oxide semiconductor field-effect transistor (MOSFET) on the integrated circuits. The prognostic cell was accelerated to failure under certain environmental conditions. Acceleration of the breakdown of an oxide could be achieved by applying a voltage higher than the supply voltage to increase the electric field across the oxide. When the prognostics cell failed, a certain fraction of the circuit lifetime was used up. The fraction of consumed circuit life was dependent on the amount of over voltage applied and could be estimated from the known distribution of failure times.

Lall et al. [50] proposed a damage precursor-based health management and prognostication methodology to electronic systems in harsh environments, which is similar to the canary approach mentioned above. The framework has been developed based on a development of correlation between damage precursors and underlying degradation mechanisms in lead-free packaging architectures. Test vehicle includes various area-array packaging architectures subjected to single thermo-mechanical stresses including thermal cycling in the range of -40°C to 125°C and isothermal aging at 125°C . Experimental data on damage precursors has been presented for packaging architectures encompassing flex-substrate ball grid arrays, chip-array ball grid arrays, and plastic ball grid arrays. Examples of damage proxies include phase-

growth parameter, intermetallic thickness and interfacial stress variations. Damage proxies have correlated with residual life.

2.3 Prognostics implementation procedure

The PoF methodology is founded on the premise that failures result from fundamental mechanical, chemical, electrical, thermal and radiation processes. The objective of the PoF methodology in the prognostics process is to calculate the cumulative damage accumulation due to various failure mechanisms for a product in a given environment. The approach (shown in Figure 1 [6]) consists of design capture, life cycle loading monitoring, failure modes, mechanisms, effect analysis, and reliability assessment.

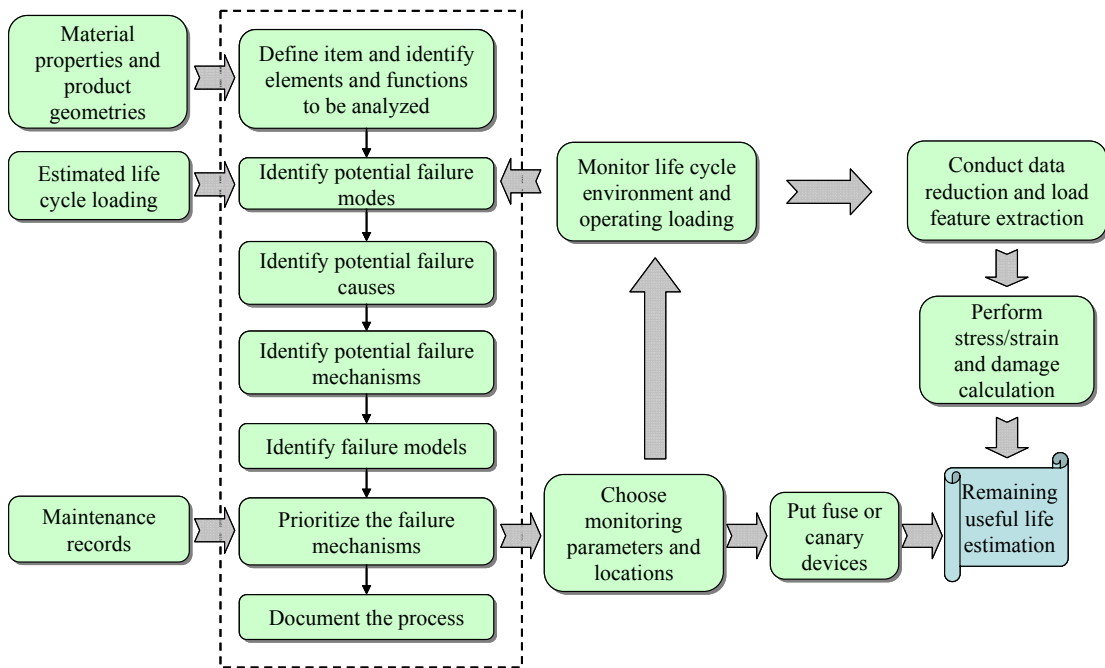


Figure 1. PoF-based prognostics approach

Design capture is the process of collecting structural (dimensional) and material information about a product to generate a model [31]. This step involves characterizing the product at all levels, i.e., parts, systems, as well as physical interfaces.

The life-cycle environment of a product consists of manufacturing, shipment, storage, handling, operating and non-operating conditions. The life-cycle loads (thermal, mechanical, chemical, electrical and so on) may lead to performance or physical degradation of the product and may reduce its service life [42]. The extent and rate of product degradation depends on the magnitude and duration of exposure (usage rate, frequency, and severity) of such loads. If one can measure these loads in situ, the load profiles can be used in conjunction with damage models to assess the degradation due to cumulative load exposures. The typical life cycle loads have been summarized in Table 1 [45].

Table 1. Life cycle loads

Load	Load Conditions
Thermal	Steady-state temperature, temperature ranges, temperature cycles, temperature gradients, ramp rates, heat dissipation
Mechanical	Pressure magnitude, pressure gradient, vibration, shock load, acoustic level, strain, stress
Chemical	Aggressive versus inert environment, humidity level, contamination, ozone, pollution, fuel spills
Physical	Radiation, electromagnetic interference, altitude
Electrical	Current, voltage, power

Experience has shown that even the simplest data collection systems can accumulate vast amounts of data quickly, requiring either a frequent download procedure or a large capacity storage device [51]. The main reasons for using data reduction in life consumption monitoring are: reduction of storage space; reduction in data-logger CPU load; and alignment with life prediction models. The efficiency measures of data reduction methods should consider: gains in computing speed and testing time; the ability to condense load histories without sacrificing important damage characteristics; and estimation of the error introduced by omitting data points.

Vichare et al. [52] has studied the accuracy associated with a number of data reduction methods such as: ordered overall range (OOR), rainflow cycle counting, range-pair counting, peak counting, level crossing counting, fatigue meter counting, range counting, etc.

Embedding the data reduction and load parameter extraction algorithms into the sensor modules as suggested by Vichare et al. [52] can lead to a reduction in on-board storage space, lower power consumption, and uninterrupted data collection over longer durations. As shown in Figure 2, a time-load signal can be monitored in situ using sensors, and further processed to extract (in this case) cyclic range (Δs), cyclic mean load (S_{mean}), rate of change of load (ds/dt), and dwell time (t_D) using embedded load extraction algorithms. The extracted load parameters can be stored in appropriately binned histograms to achieve further data reduction. After the binned

data is downloaded, it can be used to estimate the distributions of the load parameters. This type of output can be readily input into fatigue damage accumulation models.

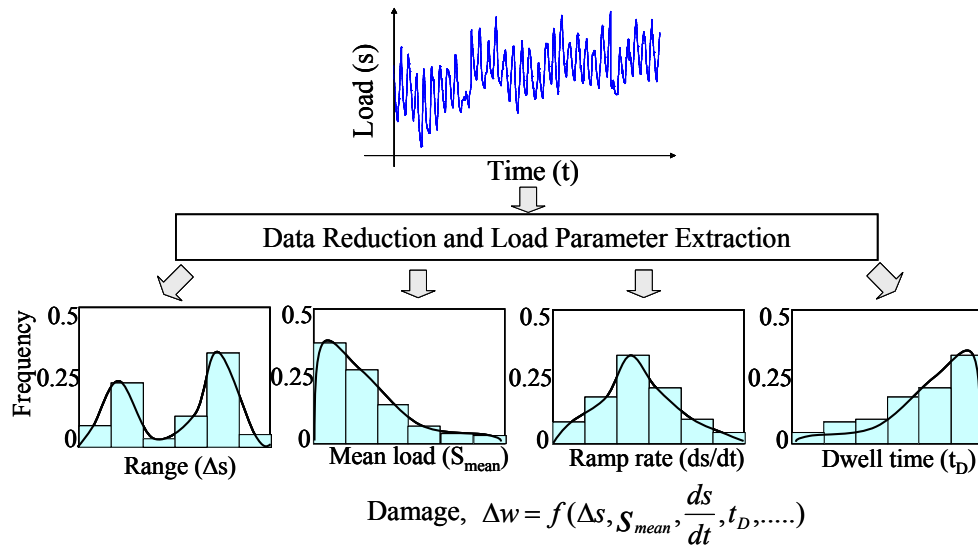


Figure 2. Load feature extraction

In Vichare's study [40][52], the temperature data was processed using two algorithms: (1) ordered overall range (OOR) to convert an irregular time-temperature history into peaks and valleys and also to remove noise due to small cycles and sensor variations, and (2) a three-parameter rainflow algorithm to process the OOR results to extract full and half cycles with cyclic range, mean and ramp rates. The approach also involved optimally binning data in a manner that provides the best estimate of the underlying probability density function of the load parameter. The load distributions were developed using non-parametric histogram and kernel density estimation

methods. The use of the proposed binning and density estimation techniques with a prognostic methodology were demonstrated on an electronic assembly.

In the FMMEA, failure modes are the effects by which a failure is observed to occur [53]. Failure mechanisms are the physical, chemical, thermodynamic, or other processes that result in failure. The failure mechanisms for electronics can be related to corresponding loads, and they are summarized in Table 2 [54]. Failure models help quantify the failure through evaluation of time-to-failure or likelihood of a failure for a given geometry, material construction, environmental and operational condition.

Table 2. Failure mechanisms, relevant loads, and models for electronics

Failure Mechanisms	Failure Sites	Relevant Loads	Failure Models
Fatigue	Die attach, Wirebond/TAB, Solder leads, Bond pads, Traces, Vias/PTHs, Interfaces	ΔT , T_{mean} , dT/dt , dwell time, ΔH , ΔV	Nonlinear Power Law (Coffin- Manson)
Corrosion	Metallizations	M , ΔV , T	Eyring (Howard)
Electromigration	Metallization	T , J	Eyring (Black)
Conductive Filament Formation	Between Metallizations	M , ∇V	Power Law (Rudra)
Stress Driven Diffusion Voiding	Metal Traces	S , T	Eyring (Okabayashi)
Time Dependant Dielectric Breakdown	Dielectric layers	V , T	Arrhenius (Fowler- Nordheim)
Δ : Cyclic range ∇ : gradient	V : Voltage M : Moisture	T : Temperature J : Current density	S : Stress H : Humidity

The reliability assessment step involves identification of appropriate PoF models for the identified failure mechanisms. A load-stress analysis is conducted using material properties, product geometry, and the life cycle loads. With the computed stresses and the failure models, an analysis is conducted to determine the cycles to failure and then the accumulated damage is estimated using a damage model.

2.4 Uncertainty studies on prognostics

Vichare et al. [55] studied the sources of uncertainty in the prognostic approach based on temperature loading condition. It was found that given the measurement, and parameter uncertainties, the actual failures in testing were observed within the predicted failure distribution. The sensitivity analysis procedure revealed that it is important to consider the standard deviation of parameter variables for calculating sensitivity indices, as it can strongly influence the ranking of the most sensitive variables.

Wu et al. [56] identified the critical parameters that influence the global/local model in solder joint reliability assessment. In their study, it is assumed that the model is correct and uncertainties are only due to variations in inputs. A global model focused on the board response, and a local model focused on the solder joint response. It was also found that the local stress analysis model is much more robust than the global model, yet for best accuracy the material properties and particularly the Young's modulus were identified being critical.

Engel et al. [57] studied how the uncertainty analysis and failure distribution could help in the condition-based maintenance for helicopter gearbox, and found the just in time (JIT) point for decision making. However no details were provided for the uncertainty analysis part.

2.5 *Summary*

Much research has been conducted on the assessment of solder joint reliability under vibration loading using the empirical, analytical, simulation, and modeling approaches. However, the amount of publications on prognostics for solder joint failure under vibration loading is very limited. In addition, all of this research has been in the frequency domain; no time domain analysis has been conducted. Only a few literatures on reliability assessment of solder joint is using in-situ vibration loading data, while in realistic the vibration loading varies a lot in different application condition. Moreover, the number of uncertainty studies for prognostics are very limited, and current uncertainty studies are limited to changes in material properties and geometries but do not include failure model uncertainty, sensor measurement uncertainty, and future usage uncertainty.

Chapter 3: In-situ Vibration Loads Monitoring for Electronic Products

The purpose of usage monitoring is to determine the actual loading conditions of a product. The life cycle profile of a product generally consists of manufacturing, shipping, storing, handling, operating, and non-operating conditions. During all those conditions, vibration load is one of the most important loads for electronic products. This chapter will give examples for in situ vibration loading monitoring.

3.1 Vibration loading monitoring for washing machine

Four accelerometers were attached to different locations at a commercial washing machine: outside the machine case, outer barrel, task control electronics and water control electronics Figure 3. The accelerometer data were collected by the Shock and Vibration Environment Recorder (SAVER). The vibration maximum G level is reported in Figure 4. As we can see, during different washing stages (for example, spinning cycle and rinse cycle), the vibration levels are not the same. Spinning generates the highest vibration loading as observed.

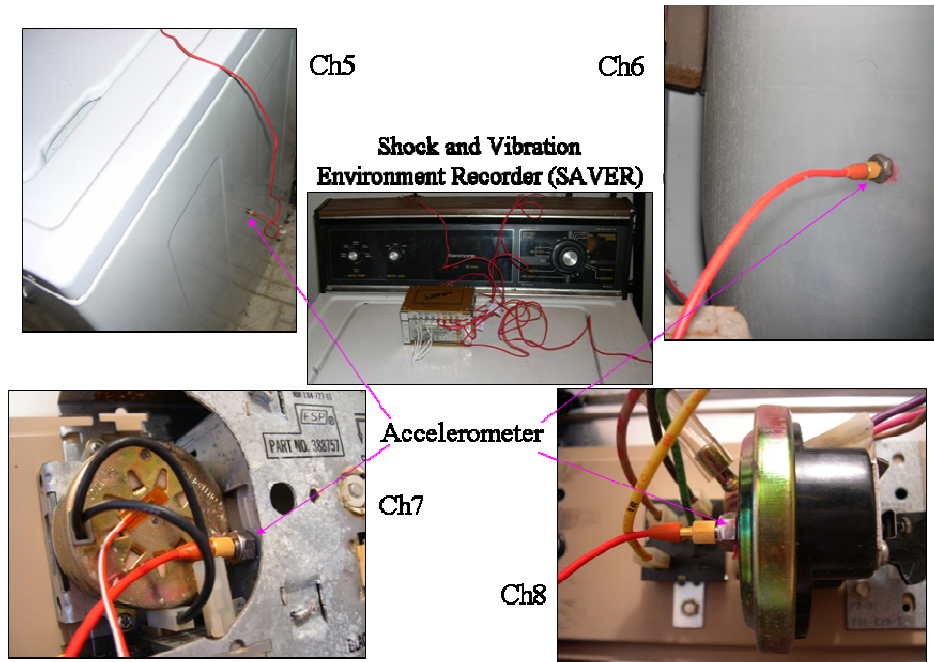


Figure 3. Vibration monitoring for washing machine – sensor locations

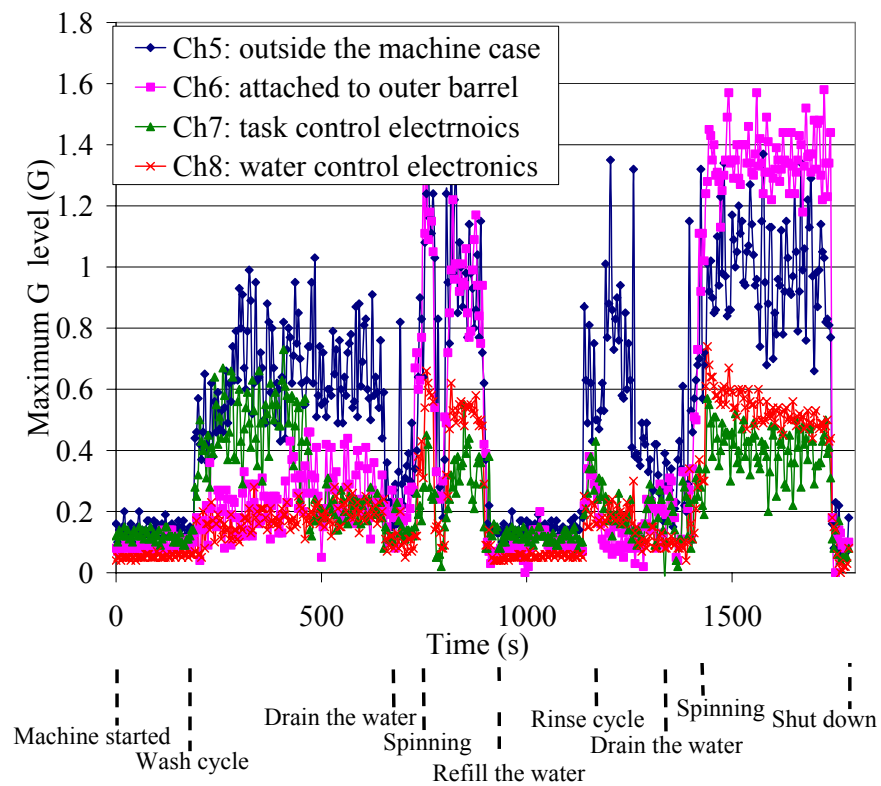


Figure 4. Vibration monitoring for washing machine – G level

3.2 *Vibration loading monitoring for notebook computer*

Vibration monitoring was also conducted on a notebook computer during transportation and use. The accelerometer was inside the express card, which was inserted into the computer, as shown in Figure 5. The vibration level (peak acceleration) was documented in Figure 6, and it showed that during different conditions (for example, transportation and use), it experienced different loading conditions. The X-axis is the trigger event ID number, and the accelerometer began recording the data when the vibration level met a preset trigger threshold. The Y-axis is the peak acceleration level for each triggered event. The first triggered event occurred when the computer (with a sensor module inside) was put in a bag and the bag was given to a user. The next trigger event occurred when the user took the bag to his car and drove home. After that, the user took the computer out of the bag and used it for half an hour, triggering the sensor module. The next morning, when the user drove back to the campus, the sensor module was also triggered. Even in the same transportation route, the vibration level (Grms) is not the same, as shown in Figure 7. In Figure 7, the height of the red bubble indicates the vibration level.

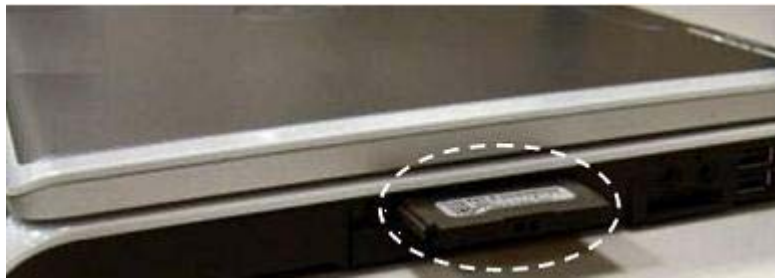


Figure 5. Sensor location for vibration monitoring of notebook computer

Further experiments were conducted. Figure 8 shows one day's usage monitoring of vibration for ten different computer users (home and office user). Figure 9 shows the vibration monitoring during use by a single user over six days. Peak acceleration and Grms value were documented. Analysis of variance (ANOVA) tests [58] were conducted. ANOVA is the method used to test for differences among different groups of data. It was observed that the vibration loading level changed from person to person. Even for a given person, the vibration loading level changed from time to time. These results were expected, since different users exhibit different behaviors with regard to the use of products over time.

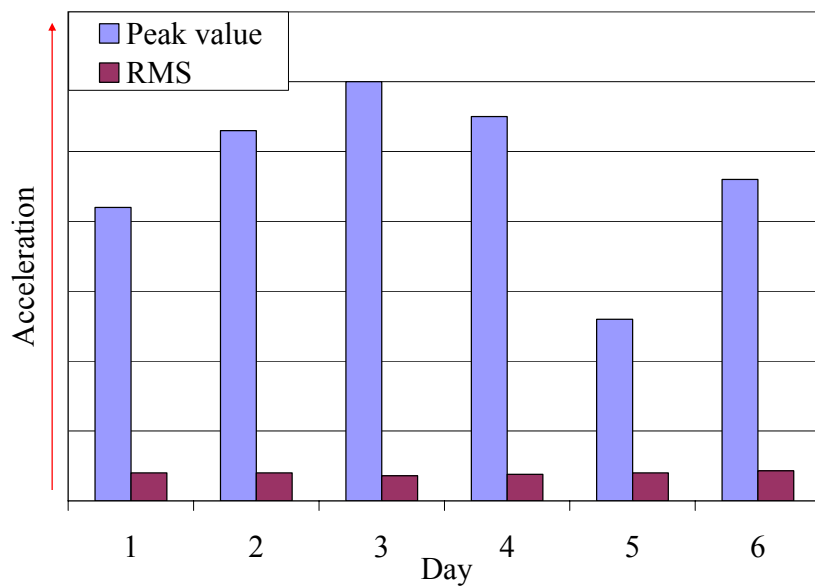


Figure 8. Vibration variation for a single user during different days

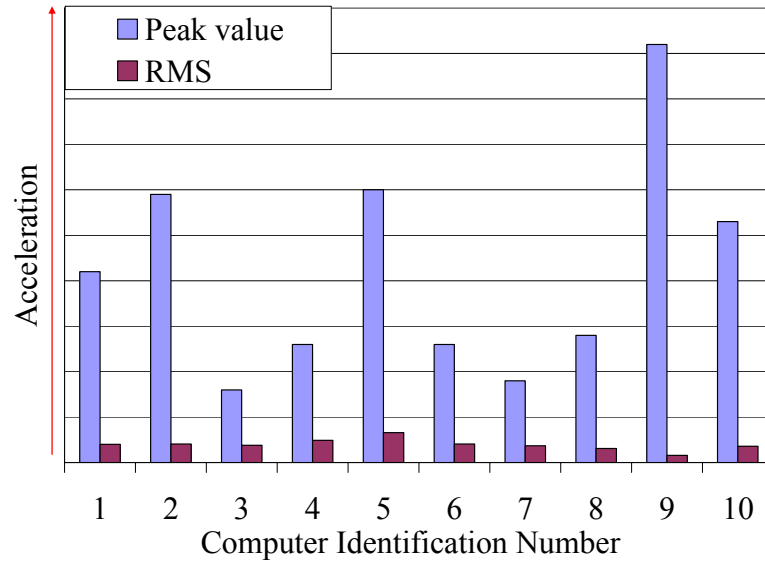


Figure 9. One day’s vibration variation for ten computers with different users

3.3 Summary

The vibration loading of a product changes from user to user and from time to time. Obtaining the real usage loading is very important for in-situ reliability assessment, since the loading condition is the key factor that contributes to product life consumption. In-situ monitoring provides a way to get a real usage profile of a product from different populations of users at different time periods.

Chapter 4: Prognostics and Health Management of Electronics under Vibration loading

Field failures of electronic equipment related to their operating environment show that about 55% of the failures are due to high temperatures and temperature cycling, 20% of the failures are related to vibration and shock, and 20% are due to humidity [18]. Prognostics methods for electronics under thermal loading have been summarized by Vichare [59]. This chapter will address the prognostics methods for electronics under vibration loading. Therefore, the experiments are designed such that vibration is the dominant factor.

4.1 Prognostics approach for electronics under vibration loading

The overall approach of prognostics for electronics under vibration loading is shown in Figure 10. First, a virtual qualification tool, such as calcePWA software, was used to quickly assess the printed circuit board (PCB) assembly. Since some complicated PCBs have hundreds of components, it is essential to identify those most likely to fail. The results revealed that solder joint vibration fatigue failure was the dominant failure model. The software also identified the natural frequency of the PCB and the locations of critical components at certain vibration loading levels. In this study, both strain gauges and an accelerometer were put on the board in order to measure its vibration response. Next, the PCB vibration response (PCB acceleration

and PCB strain) was converted into solder stress by using modal analysis and finite element analysis. After that, the failure fatigue model and the damage accumulation model were used to assess the accumulated damage. Based on that analysis, the reliability (the remaining life) of the components on the board was assessed.

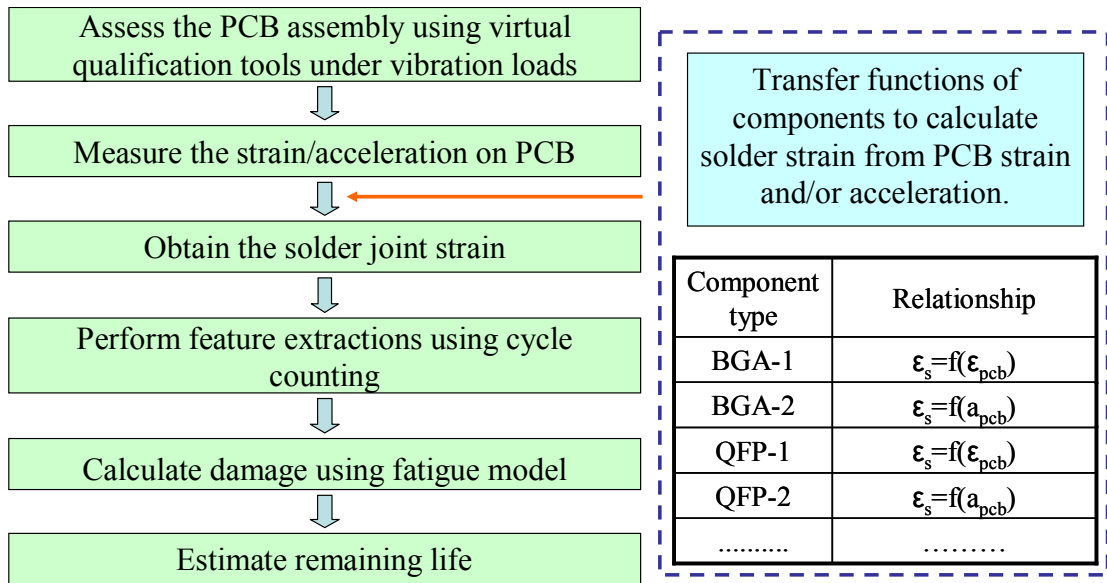


Figure 10. The prognostics approach for electronics under vibration loading

4.1.1 Characterization of the test board

The board used for demonstration of prognostics approach is shown in Figure 11. It has six ball grid array (BGA) components and six quad flat package (QFP) components. For each BGA, it has four daisy chains, and for each QFP, it only has one daisy chain. All components are mounted on one side of PCB.

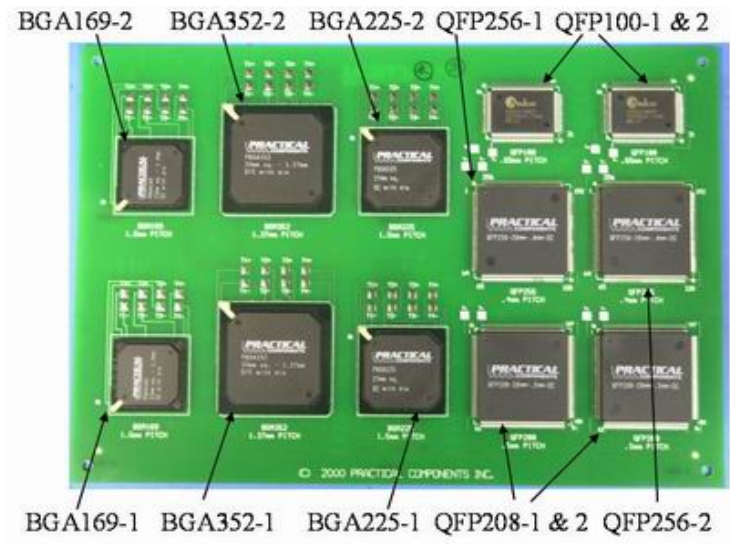


Figure 11. Test board for demonstration of prognostics under vibration

The calcePWA software was used to calculate the natural frequency of the board, and the results were compared with experiment results (see Table 3). The largest displacement occurred in the middle of the board and was found to be proportional to the stress level of the interconnect. This is also according to Steinberg’s model [18].

Table 3. Natural frequency of the test board

Natural frequency (Hz)	First mode	Second mode	Third mode
calcePWA result	108	193	332
Experiment result	108	181	317

4.1.2 Transfer function from PCB strain/acceleration to solder strain

While solder stress is the factor of interest, it is not possible to measure it directly. This is one of the challenges for assessing the reliability of electronics, since their scale is smaller than most sensors. Although micro-electromechanical systems (MEMS) are available, they are still expensive and not easy to use. Therefore, this study measured PCB response (PCB acceleration and PCB strain) and then converted them to solder stress.

4.1.2.1 PCB strain to solder strain

First, a local finite element analysis (FEA) model was built to obtain the strain in the corner solder joint and the strain on the back side of the PCB during bending, as shown in Figure 12. The corner solder joint is more critical one than any other joints in the FEA results, including the joint underneath the corner of the die. Secondly, the relationship of PCB strain and solder strain was plotted, and a linear curve was used to fit it (Figure 13). The purpose of using a linear relationship was to calibrate the analytical approach later.

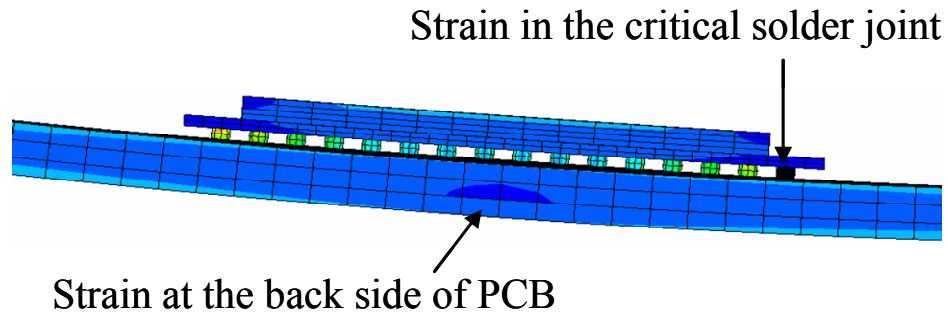


Figure 12. Local FEA analysis for strain transfer function

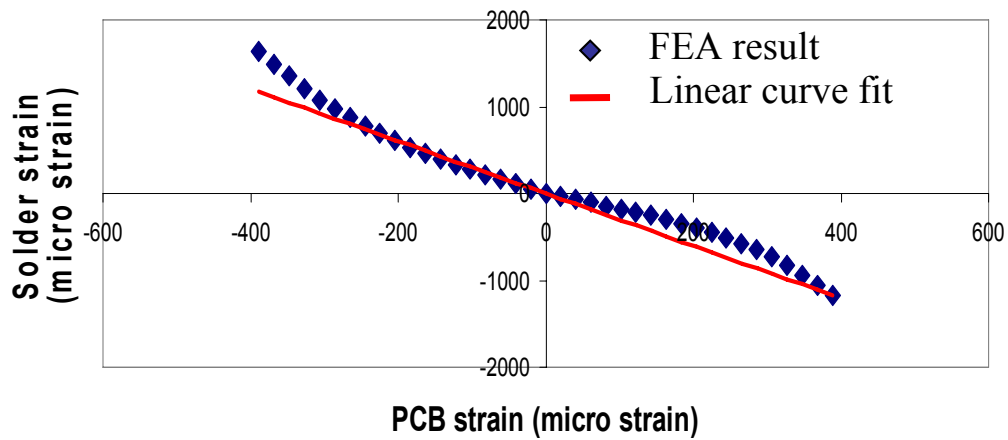


Figure 13. Strain relationship between PCB strain and solder strain

The analytical approach that was used was based on Chen's model [60]. The assumption of this approach is that the local PCB bending curvature remains constant. The 2D model for a ball grid array (BGA) component is shown in Figure 14.

$$\delta_0 = \frac{1}{m} \sum_{i=1}^m Z_i \quad (4-3)$$

$$\delta_i = \delta_0 - z_i \quad (4-4)$$

$$\varepsilon_{solder} = \frac{1}{\alpha} \frac{\delta_i}{H_{solder}} \quad (4-5)$$

$$\alpha = f(E_{solder}, D_{solder}, N_{solder}) \quad (4-6)$$

where R is curvature radius, t is PCB thickness, H is solder height, K is curvature, L is component length, x and z are the locations of each component in special directions, δ is displacement of solder joint, ε is strain, and α is the interconnect factor. E is the solder's Young's modulus, D is solder ball maximum diameter, and N is the number of solder balls on one edge. For BGA components, the interconnect factor is the function of the solder's Young's modulus, solder ball diameter, and the number of solder balls on the edge suffering the largest PCB bending curvature. Solder ball height is not included in the interconnect factor, since it has already been accounted for in Equation (4-5).

For a 3D problem (Figure 15), Equations (4-7) through (4-14) can be used. When the boundary along Y directions has been clamped, R_y will be infinite, and Z_{1j} will be 0, so the problem will revert to the 2D problem again.

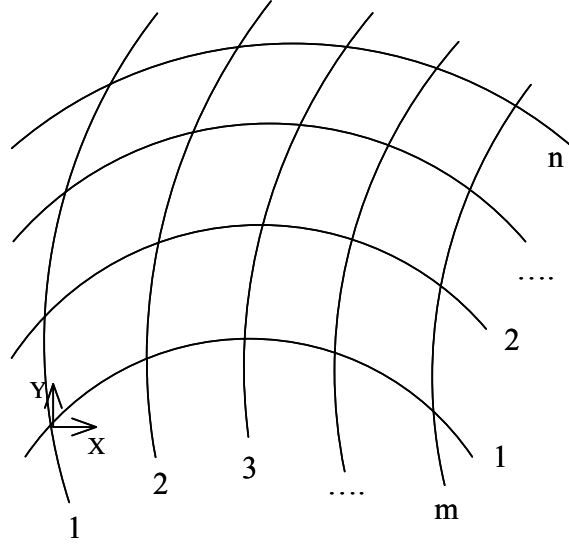


Figure 15. 3D analytical model of full grid array for strain transfer function

$$\frac{1}{R_x} = \frac{\varepsilon_{PCB-x}}{t_{PCB} / 2} \quad (4-7)$$

$$\frac{1}{R_y} = \frac{\varepsilon_{PCB-y}}{t_{PCB} / 2} \quad (4-8)$$

$$Z_{i1} = \sqrt{R_x^2 - (x_i - \frac{L_x}{2})^2} - \sqrt{R_x^2 - \frac{L_x^2}{4}} \quad (4-9)$$

$$Z_{1j} = \sqrt{R_y^2 - (x_j - \frac{L_y}{2})^2} - \sqrt{R_y^2 - \frac{L_y^2}{4}} \quad (4-10)$$

$$Z_{ij} = Z_{i1} + Z_{1j} \quad (4-11)$$

$$\delta_0 = \frac{1}{mn} \sum_{i=1}^m \sum_{j=1}^n Z_{ij} \quad (4-12)$$

$$\delta_{ij} = \delta_0 - z_{ij} \quad (4-13)$$

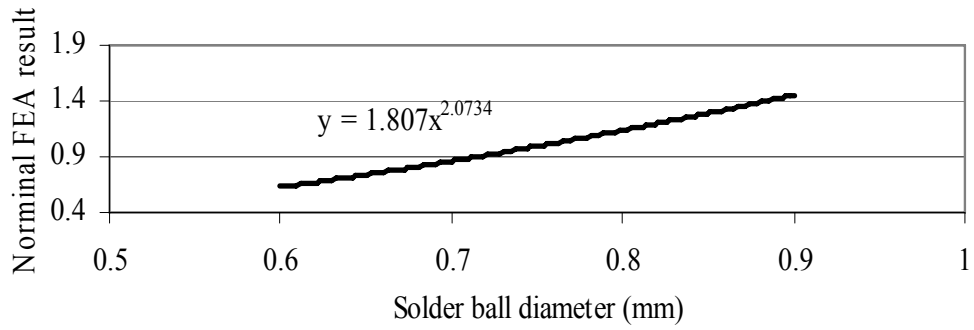
$$\varepsilon_{solder} = \frac{1}{\alpha H_{solder}} \delta_{ij} \quad (4-14)$$

For the interconnect factor α , the variables E, D, and N were assumed to be independent. As long as the solder ball diameter is less than the solder pitch, the number of solder balls along one edge of the component will not be constrained. Series of FEA analyses were carried out to evaluate the effect of E, D, and N (Figure 16). By evaluating or changing one parameter at a time, leaving the other two parameters the same, it was ascertained how the parameter contributed to the solder strain and PCB strain relation. This was repeated three times, determining the effects of all three parameters.

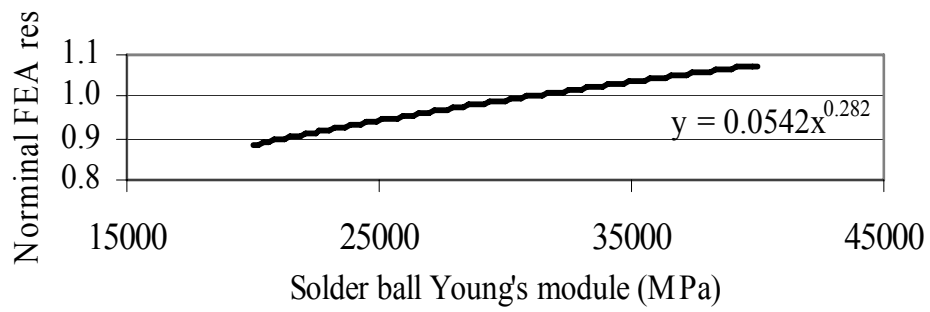
For example, in Figure 16, the X-axis represents the change in the parameters, and the Y-axis shows the nominal value of the solder strain and PCB strain relation. The power line curve was used to represent the parameter effect. Then BGA169 was used as a base line to compare the analytical approach with the FEA result (linear curve fit relation), and got the final interconnect factor shown in Equation (4-15).

$$\varepsilon_{solder} = \frac{1}{3.83 \left(\frac{D_{solder}}{0.76} \right)^{2.07} \left(\frac{E_{solder}}{29914} \right)^{0.28} \left(\frac{N_{solder}}{13} \right)^{2.63}} \delta_i H_{solder} \quad (4-15)$$

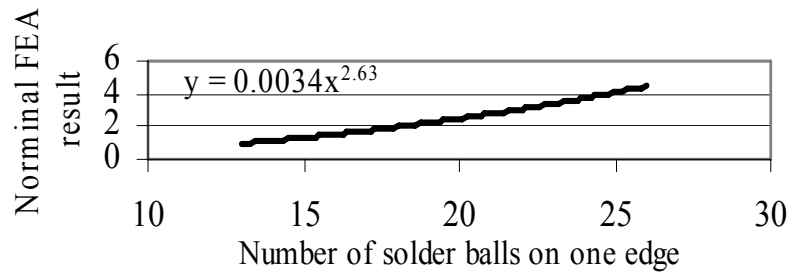
The interconnect factor was then used to calculate the relationship between PCB strain and solder strain for BGA225 and BGA352. The analytical approach results were compared with the FEA results shown in Table 4.



(a)



(b)



(c)

Figure 16. Interconnect factor parameter estimation

Table 4. PCB strain and solder strain relationship for BGA components

	BGA169	BGA225	BGA352
Component length (mm)	23	27	35
BGA span (mm)	18	21	31.75
Number of solder balls on one edge	13	15	26
PCB thickness (mm)	1.829	1.829	1.829
Solder ball pitch (mm)	1.5	1.5	1.27
Solder ball height (mm)	0.52	0.52	0.52
Solder ball diameter (mm)	0.76	0.76	0.76
Solder ball Young's modulus (MPa)	29914	29914	29914
Analytical result ($\epsilon_{\text{solder}} / \epsilon_{\text{PCB}}$)	13.58	12.86	7.15
FEA result (ABAQUS linear fit curve)	13.58	11.82	7.59
Error	0.00%	8.80%	-5.80%

For QFP components, Equations (4-16) through (4-21) were used to calculate the corner interconnect displacement. The solder strain could not be calculated directly since it was a gull-wing lead, so the gull-wing stiffness in the Z direction was calculated. This could be calculated from Equation (4-22), which is a simplified equation from Kotlowitz's model [61] when only considering the stiffness in the Z direction. From the interconnect displacement and the lead stiffness, the force in the gull-wing lead was calculated, which should be the same as the force in the solder in Z direction. Dividing the solder force by the solder bond area provided the solder stress, which can be transferred to the solder strain using a material strain and stress curve.

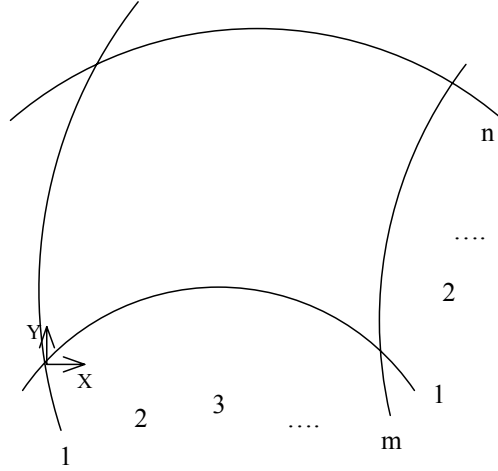


Figure 17. 3D analytical model of peripheral array for strain transfer function

$$\frac{1}{R_x} = \frac{\varepsilon_{PCB-x}}{t_{PCB} / 2} \quad (4-16)$$

$$\frac{1}{R_y} = \frac{\varepsilon_{PCB-y}}{t_{PCB} / 2} \quad (4-17)$$

$$Z_{i1} = \sqrt{R_x^2 - (x_i - \frac{L_x}{2})^2} - \sqrt{R_x^2 - \frac{L_x^2}{4}} \quad (4-18)$$

$$Z_{1j} = \sqrt{R_y^2 - (x_j - \frac{L_y}{2})^2} - \sqrt{R_y^2 - \frac{L_y^2}{4}} \quad (4-19)$$

$$\delta_0 = \frac{1}{m+n} \left(\sum_{i=1}^m Z_{i1} + \sum_{j=1}^n Z_{1j} \right) \quad (4-20)$$

$$\delta_{ij} = \delta_0 - z_{ij} \quad (4-21)$$

$$SIZ = \frac{wEt^3}{L_1 t^2 + 4L_2^3 + 2.4(1+\nu)L_2 t^2} \quad (4-22)$$

where w is the lead width, t is the lead thickness, L_1 and L_2 are the lead lengths, ν is the Poisson ratio, and SIZ is stiffness in Z direction of the gull-wing lead.

Finally, the solder strain was calculated using Equations (4-23) and (4-24).

$$\varepsilon_{solder} = f\left(\frac{1}{\alpha} \frac{\delta_i \cdot SIZ}{A_{bond}}\right) \quad (4-23)$$

$$\alpha = 0.45 \left(\frac{N_{solder}}{64} \right) \quad (4-24)$$

where α is the interconnect factor, A is the solder bond area, and f is the strain and stress relation curve for that material. The interconnect factor was calibrated by FEA results using the same approach as shown for BGA component calibration.

4.1.2.2 PCB acceleration to PCB strain

The relationship between local PCB strain and solder strain/stress has been established in the previous section. This section focuses on the global strain and acceleration measured in the middle of the PCB, since global sensor information can be used to assess the reliability of multiple components. As mentioned before, hundreds or even thousands of components can be on a single board; therefore, it is necessary to capture the global response of the board using sensors rather than perform calculations component by component using local sensor information.

In order to transfer global sensor information to local sensor information, a modal analysis (Figure 18) was conducted. The initial test and Fast Fourier Transform (FFT) analysis revealed that the first mode was dominant (Figure 19). From the first mode shape of the PCB, Equation (4-25) was gotten:

$$Z = Z_0 \left(\cos \frac{2\pi x}{a} - 1 \right) \sin(2\pi ft) \quad (4-25)$$

where x and z indicate the location shown in Figure 18, a is the PCB length along the X-axis, f is the frequency, and t is the time.

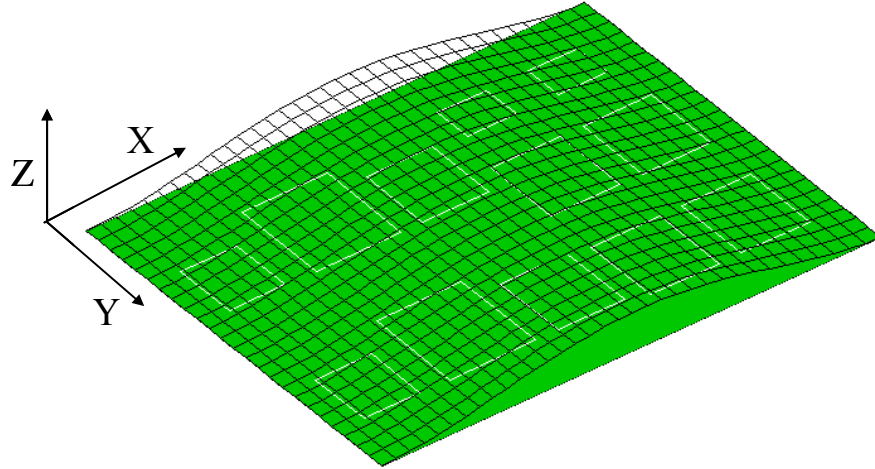


Figure 18. Modal analysis for PCB

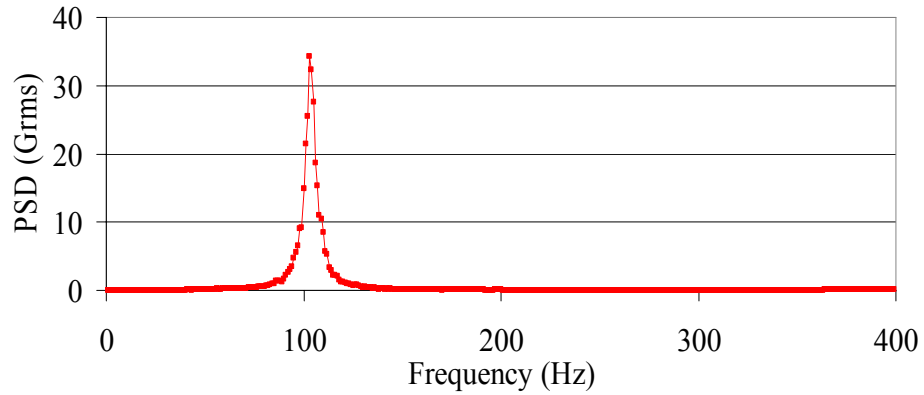


Figure 19. FFT analysis for the initial vibration test

When Equation (4-25) was differentiated twice in the time domain, we got the acceleration in the Z direction, as shown in Equation (4-26); when Equation (4-25) was differentiated twice in the X direction, we got the PCB bending curvature along the X direction, as shown in Equation (4-27).

$$Accel = Z_{tt} = -4\pi^2 f^2 Z_0 \left(\cos \frac{2\pi x}{a} - 1 \right) \sin 2\pi ft \quad (4-26)$$

$$k = Z_{xx} = -Z_0 \frac{4\pi^2}{a^2} \cos \frac{2\pi x}{a} \sin 2\pi ft \quad (4-27)$$

where *Accel* is the PCB acceleration in the Z direction, and *k* is the PCB bending curvature along the X direction.

The relationship between the PCB bending curvature and the PCB strain is shown in Equation (4-28). After combining Equations (4-26) and (4-28), the relationship between the PCB acceleration and the PCB strain was gotten, as shown in Equation (4-29):

$$k = \frac{\varepsilon_{PCB}}{t_{PCB}/2} \quad (4-28)$$

$$\varepsilon_{PCB} = \frac{t_{PCB} \cos \frac{2\pi x}{a}}{2a^2 f^2 \left(\cos \frac{2\pi x}{a} - 1 \right)} Accel \quad (4-29)$$

where ε_{PCB} is the PCB strain and t_{PCB} is the PCB thickness. When comparing the ε_{PCB} value in the middle of the PCB, the ratio between the experimental measurement value and the calculated value (from Equation (4-29)) using the measured acceleration value was 1.18. This indicated that it was possible to use an accelerometer to capture board response. In addition, an accelerometer, in terms of its installation and associated signal conditioning circuitry, is simpler, cheaper, and more reliable than strain gauges.

From Equation (4-26), the acceleration relationship from different locations on the PCB was obtained, as shown in Equation (4-30):

$$\frac{Accel_1}{Accel_2} = \frac{\cos \frac{2\pi x_1}{a} - 1}{\cos \frac{2\pi x_2}{a} - 1} \quad (4-30)$$

where $Accel_1$ and $Accel_2$ represent the acceleration in x_1 and x_2 locations, respectively. Therefore, the measured acceleration (in the middle of the PCB) was able to be transferred to any local area. Then Equation (4-29) was used to calculate local PCB strain.

After global acceleration or strain was converted into local PCB strain, it was necessary to consider the strain relationship between boards with and without components. Since the components add to the stiffness of the board, they will affect local PCB strain. Finite element analysis (FEA) was conducted, as shown in Figure 20. From that, the ratio between these two strains was calculated.

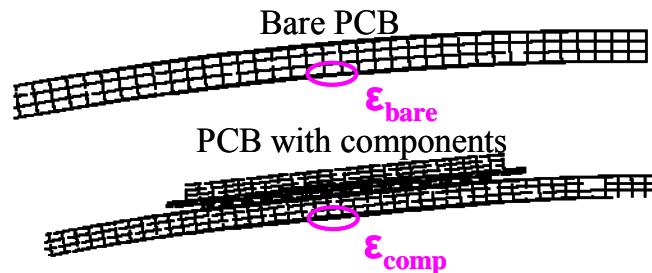


Figure 20. Strain relationship between boards with and without components

4.2 Equipment setup and process

4.2.1 Vibration shaker setup

The test board was mounted on the vibration shaker using two-edge-clamped boundary condition as shown in Figure 21. The shaker could excite the vibration in the out-of-plane direction. The step stress test was carried out as shown in Table 5. In each step the loading condition was random vibration loading with frequency response from 40Hz to 500Hz (Figure 22). Before the step stress test, one board was also used to carry out the initial test, such as natural frequency analysis. From the initial test, it was known that the strain along the length of PCB is much higher than the strain along the width of the PCB. Therefore, the later one could be neglected in the test. In addition, the noise of the sensor under no loading condition was also analyzed. The strain range within noise level would be filtered out during the cyclic counting of the step stress monitoring data, since they will not count for the damage calculation.



Figure 21. Test board mounted on the vibration shaker

Table 5. Vibration step stress test matrix

Step	PSD level (G ² /Hz)	Duration (hours)
1	0.05	5
2	0.1	5
3	0.2	5
4	0.3	6

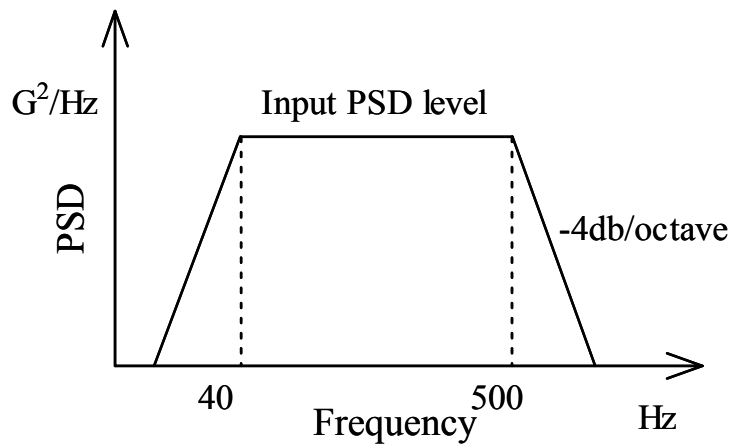


Figure 22. Random vibration loading input profile

4.2.2 Sensor location and data acquisition setup

The strain gauges were mounted on the back side of the PCB (shown in Figure 23). They were right underneath the components. The strain data were collected by the NI SCXI1314 data acquisition card incorporated with the Labview program. The accelerometer was mounted in the middle of the front side of the PCB (shown in Figure 21). The acceleration data were collected by the Shock and Vibration Environment Record (SAVER). Both the Labview program (for strain measurement) and SAVER (for acceleration measurement) were coded to have both the time triggered and signal triggered functions. For the time trigger situation, the program recorded 1024 data points every minute with a 1024 Hz sampling frequency. For the signal trigger situation, the program recorded 1024 data points (1024 Hz sampling frequency), including 5% pre-trigger data when the signal met the threshold. The threshold was set to be 90% of the maximum value in the initial test. The time trigger function was used to catch the loading distribution, while the signal trigger function was used to catch an abnormal stress condition, such as a sudden shock, during the interval of the time trigger function. The purpose for time- and signal-triggered recording rather than continual monitoring is that in continual monitoring more than 10,000 data points (from all sensors) are collected every second. This can cause difficulties for data storage and processing.

combined trigger recording were documented in Appendix A. When comparing with the sum of cycle range (SCR), the discrepancy is also with 4% (Table 6). The SCR is calculated using following equation [62]:

$$SCR = \sum cycle_range * No._of_occurrence \quad (4-31)$$

This concept is similar to Miner's rule [63], in which the total damage is a linear superposition of damage at different load levels. SCR is the linear superposition of the loading cycle range times its occurrence number at different loading levels. The details for transferring the time domain signal to cycle information is documented in Appendix B. Using SCR we can consider the effect of different environmental loading cycles together at the same time. The reason to select the loading cycle range as the loading feature in this study is because in many fatigue models (such as the Coffin-Manson model [63]) cycle range is the key input to calculate the time/cycles to failure.

In Table 6, it is also observed that the combined trigger signal is a little worse than the time triggered signal. This is because during the lab test, vibration shaker was used to conducted the experiment, therefore the vibration generated is following the normal distribution, and not totally random. In order to verify the affectivity of the combined trigger recording technology, the road test was also conducted. During the road test, the SAVER was put in the trunk of the car during the on campus during. Table 7 shows the result comparison. As can be seen in this case, the combined trigger recording provides the better accuracy.

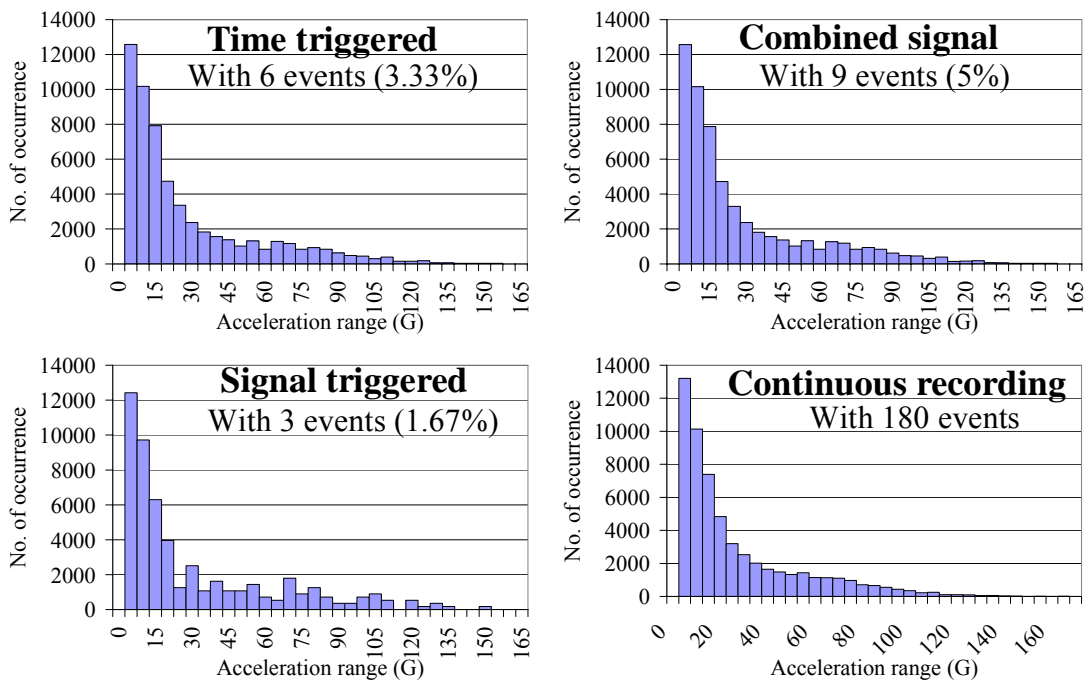


Figure 24. Combined trigger signal recording

Table 6. Signal recording method comparison for lab test data

	Time triggered	Signal triggered	Combined signal
Correlation factor	0.998	0.986	0.998
Sum of cycle range discrepancy	3.57%	7.02%	3.67%

Table 7. Signal recording method comparison for road test data

	Time triggered	Signal triggered	Combined signal
Correlation factor	0.957	0.918	0.959
Sum of cycle range discrepancy	-10.58%	12.34%	-5.9%

The initial tests were also conducted. One purpose is to get the threshold (90% of the maximum value) for the signal triggered recording. The other purpose is to get the noise level for the test. When the noise was filtered, the signal became clearer as seen in Figure 26.

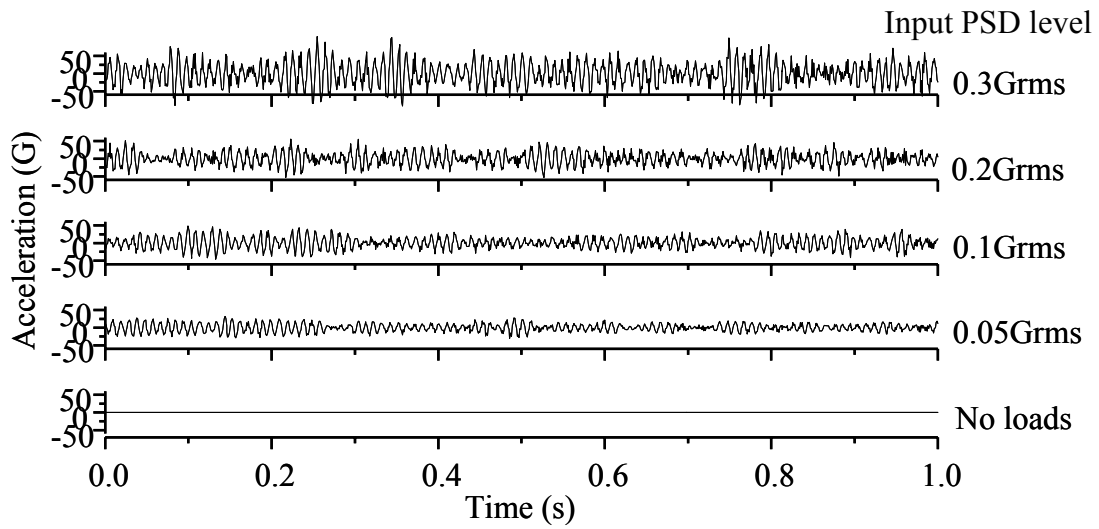
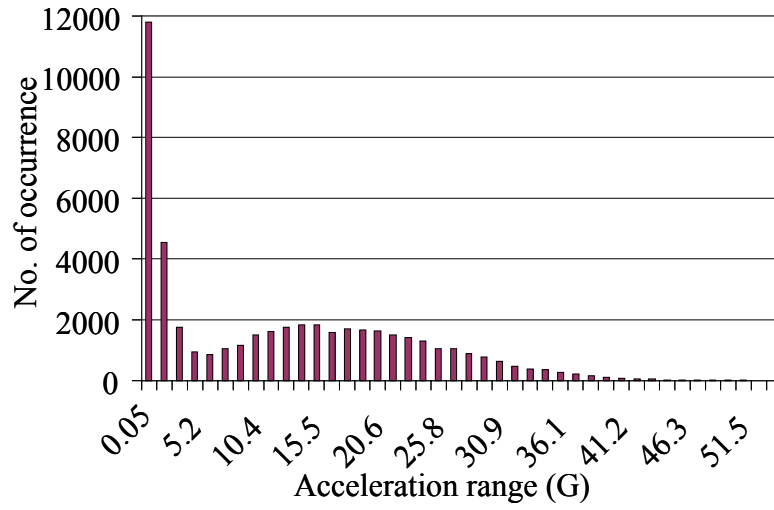
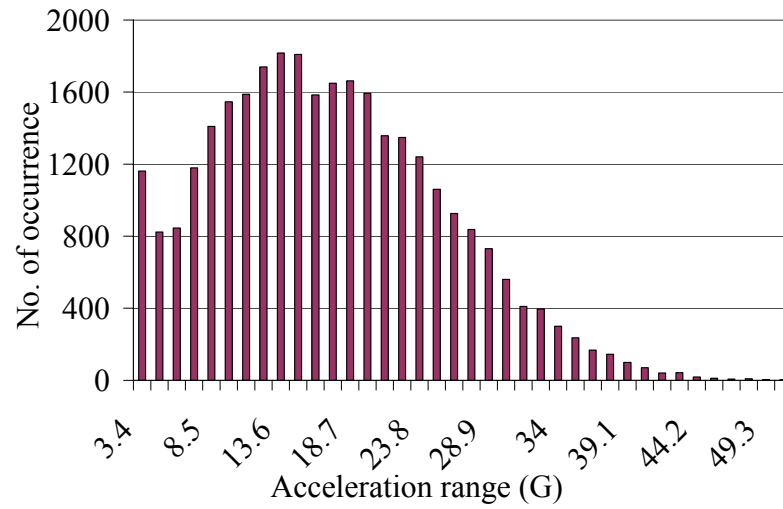


Figure 25. Initial tests for vibration tests



(a) With noise



(b) Without noise

Figure 26. Vibration acceleration histogram comparison

4.2.3 Resistance measurement

Resistance of each component was measured through daisy chain which connects to the data-logger. The data-logger monitored the resistance in situ. The failure criteria in this test were defined as: the daisy chain resistance is over 50 Ohms (1st spike), and repeats similar behavior 9 more times in the next 10% of the time to the 1st spike. When this is the case, the 1st spike is considered the time to failure point for this component. Here for the conservation purpose, 50 Ohms was chosen rather than 300 Ohms mentioned in the IPC standard [64]. For multiple daisy chains in one component, the first daisy chain failure time was considered as the component failure time.

4.2.4 Strain/acceleration transfer function verification

Before damage calculation, verification was performed to check the accuracy of calculated local PCB strain using middle PCB strain (Table 8), as well as middle PCB strain and PCB acceleration relationship (Table 9). The calculated strain values matched the measured strain values well. The location listed in two tables can be referred to Figure 23 and illustration in Figure 27.

Table 8. Local PCB strain / Middle PCB strain

Location	Experiment*	Predicted
2	0.38	0.39
3	0.31	0.28
4	0.40	0.38
5	0.30	0.24
6	0.30	0.32
7	0.30	0.33
8	0.43	0.38

*The sum of cycle ranges was compared.

Table 9. Middle PCB strain / Middle PCB acceleration ($\mu\epsilon/G$)

Location	Experiment*	Predicted
1	8.52	10.13

*The sum of cycle ranges was compared.

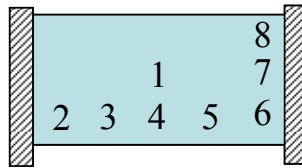


Figure 27. Sensor location illustration

4.2.5 Damage calculation and remaining life prediction

In this section, BGA352-1 was chosen as a case study to perform prognostics using the accelerometer in the middle of PCB. After the PCB acceleration values were converted into the solder stress values, cycle counting of the solder stress extracted the load feature stress amplitude. Then, the stress amplitude was binned and put into the failure fatigue model (Equation (4-32)) to obtain the time to failure for each stress amplitude level. Miner’s rule was then used to assess the accumulated

damage (Equation (4-33)). Damage is defined as the extent of a part or product's degradation or deviation from its normal operating state. The aim of damage assessment is to convert the number of cycles-to-failure values obtained from the physics-of-failure analysis into a metric for life consumption:

$$\sigma_1^b N_1 = \sigma_2^b N_2 = C \quad (4-32)$$

$$D_{total} = \sum_{i=1}^n \frac{n_i}{N_i} \quad (4-33)$$

where b and C are the material constants. The damage fraction (D) at any stress level is linearly proportional to the ratio of the number of cycles of operation (n_i) to the total number of cycles that would produce failure (N_i) at that stress level. When $D > 1$, failure is considered to have occurred. Damage was accumulated for each hour and then calculated the remaining life at each hour using Equation (4-34):

$$RL_N = \frac{N}{DR_N} - N \quad (4-34)$$

where RL_N is the remaining life at the end of N^{th} hour and DR_N is the damage ratio accumulated at the end of N hours. The history of accumulated damage and the remaining life prediction for component BGA352-1 are shown in Figure 28 and Figure 29. From Figure 29, it can be seen that the predicted remaining life was constantly changing. One reason is that the useful life was being consumed every hour; the other reason is that the loading condition changed at 5, 10, and 15 hours into the test (see Table 5). So the data in the first few hours could not accurately predict

the remaining life unless the loading condition remained the same. This explains why in situ monitoring was necessary.

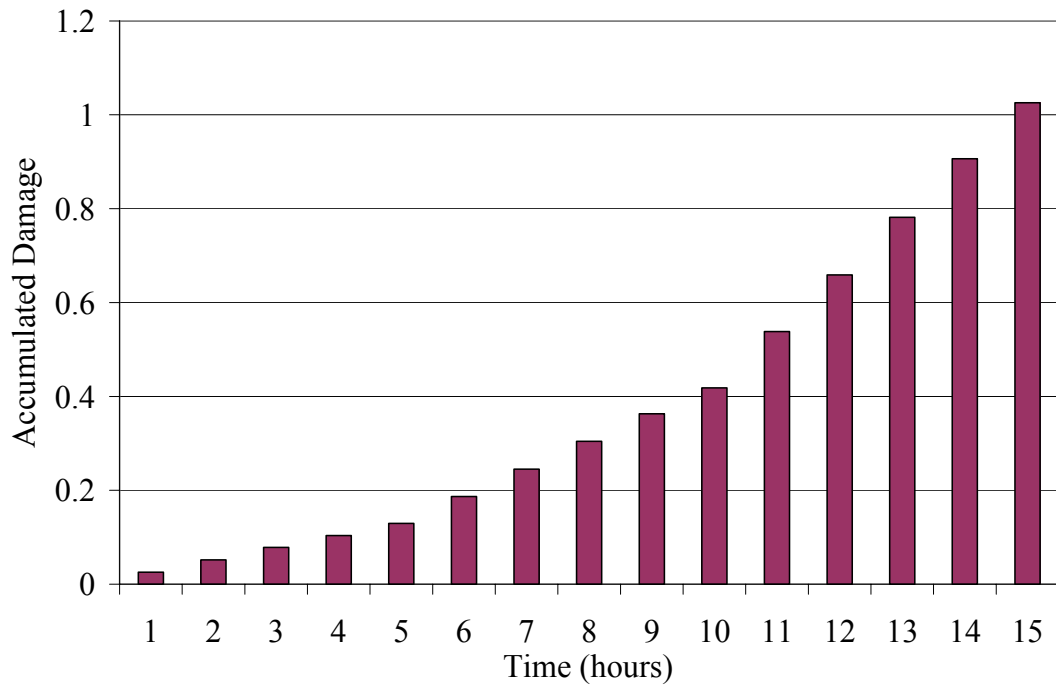


Figure 28. Accumulated damage for component BGA 352-1

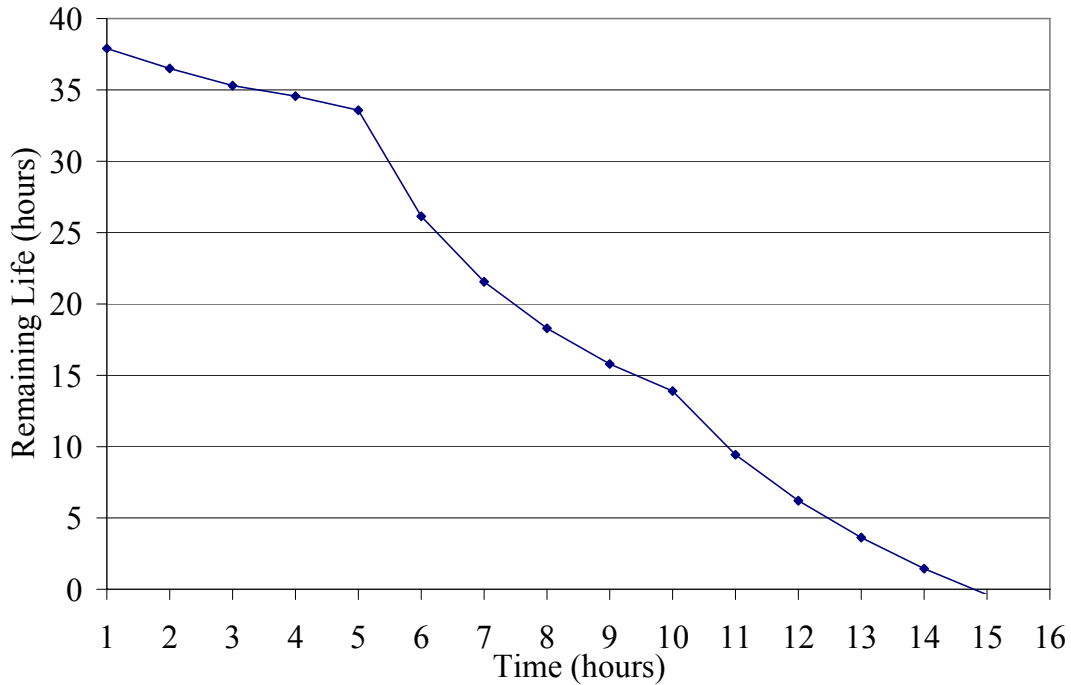


Figure 29. Remaining life prediction for component BGA352-1

A summary of other component predictions using center acceleration and experiment results is presented in Table 10. A discrepancy is defined as the ratio of experimental results to prediction results. If the experiment agreed with the prediction, the ratio is 1. If the ratio is greater than 1, it means that the component lasted longer than predicted. If the ratio is less than 1, it means that the component failed sooner than predicted. Table 10 shows that the prediction for many of the components matched very well with the experimental results. All but two of the twelve components lasted longer than predicted. Also, all but two of the components failed within a factor between 0.5 and 2 of the prediction. The two components (BGA169-1 and QFP100-2) that did not fall with 0.5 and 2 were located on opposite corners of the PCB next to the clamped edges. This implies that the PCB might not

have been behaving properly, which is exactly what the assumed theoretical boundary condition predicts for these regions. The overall prediction trend appears valid. These results were very good for the fatigue failure prediction.

Table 10. Remaining life prediction using accelerometer

Component	Time to failure (hours)		Comparison
	Experiment	Prediction	Experiment/Prediction
BGA169-1	11.36	4.52	2.51
BGA169-2	5.1	4.52	1.13
BGA225-1	5.85	5.67	1.03
BGA225-2	10.19	5.67	1.80
BGA352-1	20.72	14.79	1.40
BGA352-2	15.54	14.79	1.05
QFP100-1	5.54	8.97	0.62
QFP100-2	0.13	5.06	0.03
QFP208-1	10.01	9.19	1.09
QFP208-2	10.57	6.03	1.75
QFP256-1	15.14	11.82	1.28
QFP256-2	12.88	7.9	1.63

Reliability assessment (remaining life prediction) was also conducted using a local strain gauge and global strain information (strain in the middle of the PCB). These sensors' predictions are compared in Figure 30. If the prediction agrees perfectly with experiment, the data points will lie along a line with a slope of 1. Error bars +/-2 and +/-4 are also shown in the figure, and most data fall in the +/-2 zone. +2X means predicted life is two times as the measured life; -2X means predicted life is half of the measured life; +4X means predicted life is four times as the measured life; -4X means predicted life is a quarter of the measured life. It is also observed for some cases that the central strain/acceleration gave a better prediction than local strain. This is because the local strain measurements are more affected by the

components nearby and by the sensor's own location on the board. In addition, these data reveal that the global sensor (middle PCB strain or acceleration) information enhanced prognostics capability and can be used to monitor the status of a component that does not have local monitoring sensors.

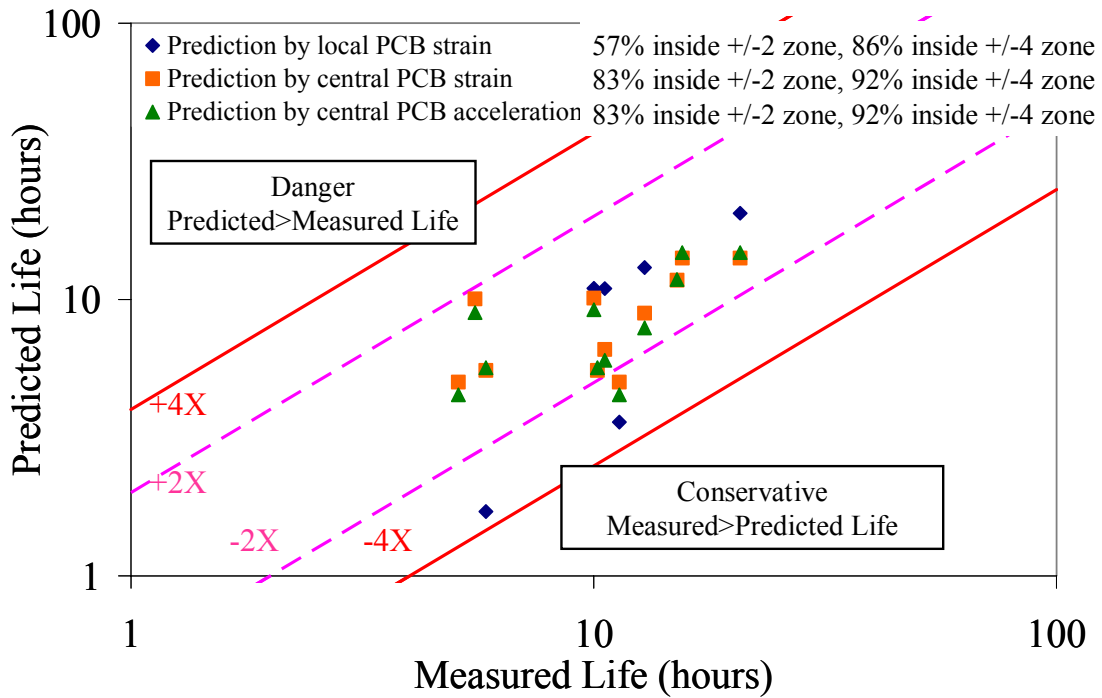


Figure 30. Comparison of remaining life prediction using different sensors

4.3 Summary

This chapter has presented a prognostics approach for assessing the reliability of solder joints under vibration loading using strain and acceleration information measured directly on a PCB. Two specific challenges for prognostics of electronics have been discussed in this chapter. One challenge is that sensors cannot be used to directly measure the loading condition of critical areas (such as solder joints) of

electronics, since the electronic components are small in scale. In the case study, the relationship between board local response and interconnect stress was obtained using FEA and an analytical approach. Therefore, it is possible to obtain the interconnect stress by measuring the local board response (acceleration or strain). The second challenge is that normally a single board has a large number of components. In the case study, the relationship between acceleration at different locations on the PCB was established by modal analysis. In addition, the relationship between PCB acceleration and PCB strain was also established. Therefore, it is possible to use global board response (at the middle of the board in this case) to estimate local board response (a specific component area of the board). A reliability assessment of the components/interconnects can then be performed.

The methodology also enables the calculation of the damage accumulation and remaining life of multiple interconnects using only a single sensor, which does not need to be placed at a component's exact location. The prediction results matched well with the experimental results. In addition, the methodology proved that an accelerometer is suitable for prognostics, which makes the field application of prognostics much easier, since the installation and associated signal conditioning circuitry of an accelerometer is simpler, cheaper, and more reliable than a strain gauge. In addition, the data recording approach developed in this chapter reduced the amount of data around 95% while keeping the accuracy above 96%.

Chapter 5: Uncertainty Assessment of Prognostics of Solder Joints Reliability

For logistics use of prognostics, it is necessary to identify the uncertainties in the prognostic approach and assess the impact of these uncertainties on the remaining life distribution in order to make risk-informed decisions. The prognostics implementation of electronics under vibration loading has been studied in previous chapter. However, the effect of uncertainty and variability for the material properties and prediction procedures were not considered at that time. With uncertainty analysis, a prediction can be expressed as a distribution rather than a single point. The prediction can be expressed as a failure probability. This chapter will address the uncertainty analysis of prognostics for electronics under vibration loading.

5.1 Uncertainty assessment approach

The uncertainties will come into different steps of prognostics approach (see Figure 31). It was found that for different failure mechanism, there are corresponding failure models, and they need different input loads (see Table 11). When monitoring these input loads, measurement uncertainties (such as sensor data measurement) would come to play. When the input loads were put into the failure model to assess the damage, the parameter uncertainties (such as material properties and structural

geometries) and model uncertainty (such as fatigue constant) would come to play. When using damage to perform remaining life prediction, it was necessary to consider the failure criteria uncertainty and future usage uncertainty. The uncertainty assessment approach was shown in Figure 32. First, uncertainty source categorization was carried out and shown in Figure 31. Then based on the sensitivity analysis, the critical parameters could be chosen for uncertainty propagation calculation. From uncertainty propagation, it could be identified how the input uncertainties affected the model outputs. At last, based on the different failure criteria and future usage loading, the future reliability of the product could be obtained.

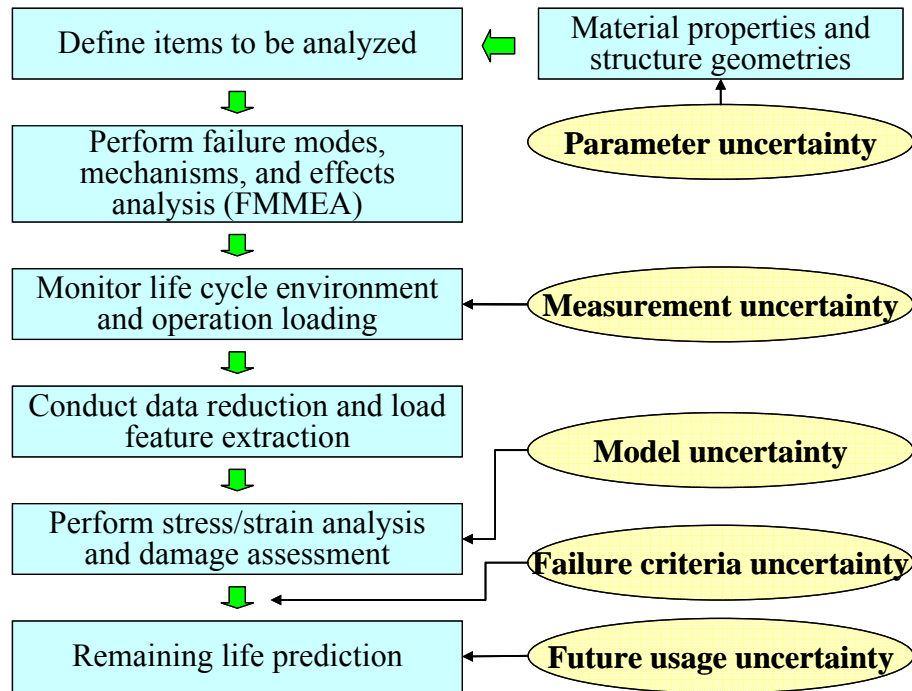


Figure 31. Uncertainty source in PoF based prognostics procedure

Table 11. Failure mechanisms, failure models, and loads

Failure Mechanism	Failure Model	Relevant Loads/Input
Fatigue (thermal)	Coffin Manson	Temperature
Fatigue (vibration)	Steinberg, Basquin	Acceleration, strain
Corrosion	Peck	Humidity, temperature
Electromigration	Black	Current density, temperature
Conductive Filament Formation	Rudra	Moisture, gradient voltage
Stress Driven Diffusion Voiding	Okabayashi	Temperature
Hot Carrier	Eyring model	Current, voltage, temperatures
Time Dependent Dielectric Breakdown	E model, 1/E model	Electric field density, voltage, temperature

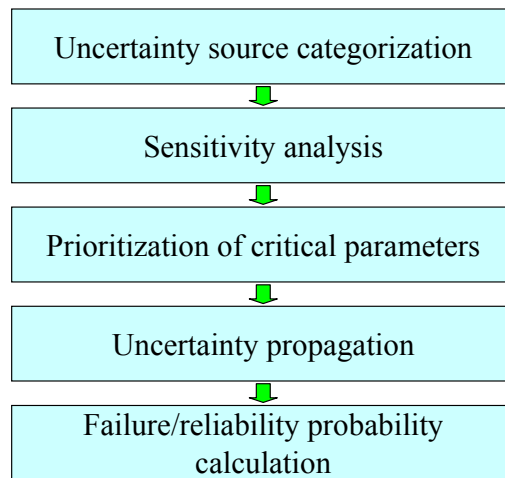


Figure 32. Uncertainty assessment approach

5.2 Uncertainty Source categorization

The experiment setup was similar to the setup in previous chapter. An electronic test board was mounted on the vibration shaker, which can excite random vibration loading. The response of the printed circuit board (PCB) to vibration

loading in terms of bending curvature was monitored using strain gauges. Then, the interconnect strain could be used in the vibration failure fatigue model for damage assessment. The damage estimates were accumulated using Miner's rule after a certain time then used to predict the life consumed and remaining life. The results were verified by real time to failure of the components by checking the components resistance data. In this study, component BGA352 (one kind of ball grid array component) was analyzed to demonstrate the uncertainty implementation approach.

Five types of uncertainties and their sources are categorized, and they are measurement uncertainty, parameter uncertainty, model uncertainty, failure criteria uncertainty and future usage uncertainty.

5.2.1 Measurement uncertainty

Measurement uncertainty can be further divided into two parts. One is sensor inaccuracy, and the other is the data reduction effect part.

The strain gauge is used in the experiment. A literature review revealed that the inaccuracy mainly comes from resistance, temperature effect, adhesive thickness, Wheatstone bridge nonlinearity, and misalignment of strain gauges. The strain gauge resistance in this study is 350 Ohm, which may have 0.3% tolerance range. In the mean time, the temperature may affect the resistance value. In the room temperature (20°C to 30°C), the effect can be 0.2% [65]. The PCB thickness is proportional to the strain measurement. So when the PCB is very thin, the adhesive thickness will become a concern. The thickness of the PCB in this test is 1.829mm, and adhesive

thickness is 0.05mm, so from a simple calculation, there can be a 2.7% error when considering the adhesive thickness. Errors due to Wheatstone bridge nonlinearity can be 0.1% when the strain level is below 1,000 $\mu\epsilon$ [66]. Misalignment will also cause strain inaccuracy. A 5° error in mounting the rosette produces a 0.68% error [67]. In our test, the adhesive did not depend on the curing temperature. When the possible errors are added together, the total is about 4% (0.3%+0.2%+2.7%+0.1%+0.68%). In addition, Vishay technique notes [68] show the error of strain gauge used in this study normally is in the range of 2% - 5%, so 4% will be the strain inaccuracy in this study.

Bin width is used for the data reduction. Smaller bin width may present too many details (undersmoothing) and larger bin widths may present too few details (oversmoothing). The optimal bin width needs to be selected. However, the optimal bin width calculation also depends on the load distribution [52]. The formulas to calculate the optimal bin width for the normal distribution and non-normal distribution [52][69] show 5% difference. This will be counted as uncertainty source when performing data reduction, since the real life loading distribution is not known in advance.

In addition, as discussed in previous chapter, by using combined trigger signal, it will generate 3.7% discrepancy, and this is also counted in the uncertainty analysis.

5.2.2 Parameter uncertainty

Parameter uncertainty considers the variation from model input, such as material properties and geometries changes. For example, in the previous chapter,

when calculating the solder strain from PCB strain, the uncertainty arises due to variability in the material and geometric parameters that are used in the stress analysis model as shown in the Equation (5-1).

$$\varepsilon_{solder} = f(\varepsilon_{PCB}, t_{PCB}, L_{BGA}, P_{BGA}, h_{solder}, D_{solder}, E_{solder}) \quad (5-1)$$

where ε_{solder} is calculated solder strain, ε_{PCB} is the measured PCB strain, t_{PCB} is the thickness of the PCB, L_{BGA} is the BGA span, P_{BGA} is the BGA pitch, h_{solder} is the height of the solder ball, D_{solder} is the solder ball diameter, and E_{solder} is the solder Young's modulus. All the uncertainties coming from these material properties or geometries will be documented and referenced in Table 12.

5.2.3 Model uncertainty

The uncertainty from the failure fatigue model arises due to the variability of the fatigue constant in the S-N curve (stress against the number of cycles to failure curve, see Figure 33).

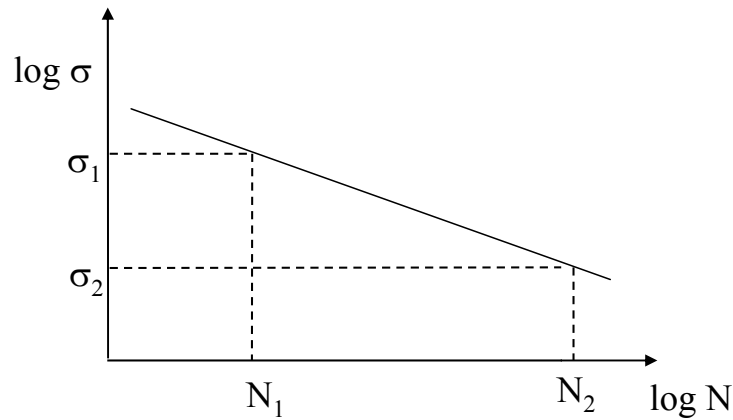


Figure 33. S-N curve

From Basquin's model,

$$\sigma_1^b N_1 = \sigma_2^b N_2 \quad (5-2)$$

where b is the fatigue constant. The slope of the S-N curve is $-1/b$.

First, we need to know the target probability in the failure prediction. It is important since many fatigue constants obtained from the literature were calculated from mean time to failure or characteristic life. However, in real application, one may only be interested in 5% failure probability time to failure. Different failure probability may have different S-N curves as shown in Figure 34 [70]. Second, one needs to be aware that the S-N curve slope for different failure probability is not the same, and that is because at different stress level, the failure probability distribution has different parameters. This can also be observed in Figure 34. It is important since much commercial software ALTA [71] and Minitab [72] assume the S-N curves for different failure probability are parallel to simplify the calculation. Third, one needs to be aware the confidence intervals for the S-N curve when fitting the line (Figure 35). In order to obtain the S-N curve, accelerated testing at different stress level should be conducted. The S-N curve will be fitted from the point of these different stress levels. From mathematical theory, the more data points, the more confidence level for the fitting with narrow confidence intervals. Therefore, one also needs to consider the confidence interval (for 95% confidence level) as the uncertainty source. From the data analysis from Figure 34, it was found that the confidence interval generates the most uncertainty, since only six data points (represents six stress levels) were used to fit the S-N curve. The fatigue constant b can change from 4.3 to 9.8.

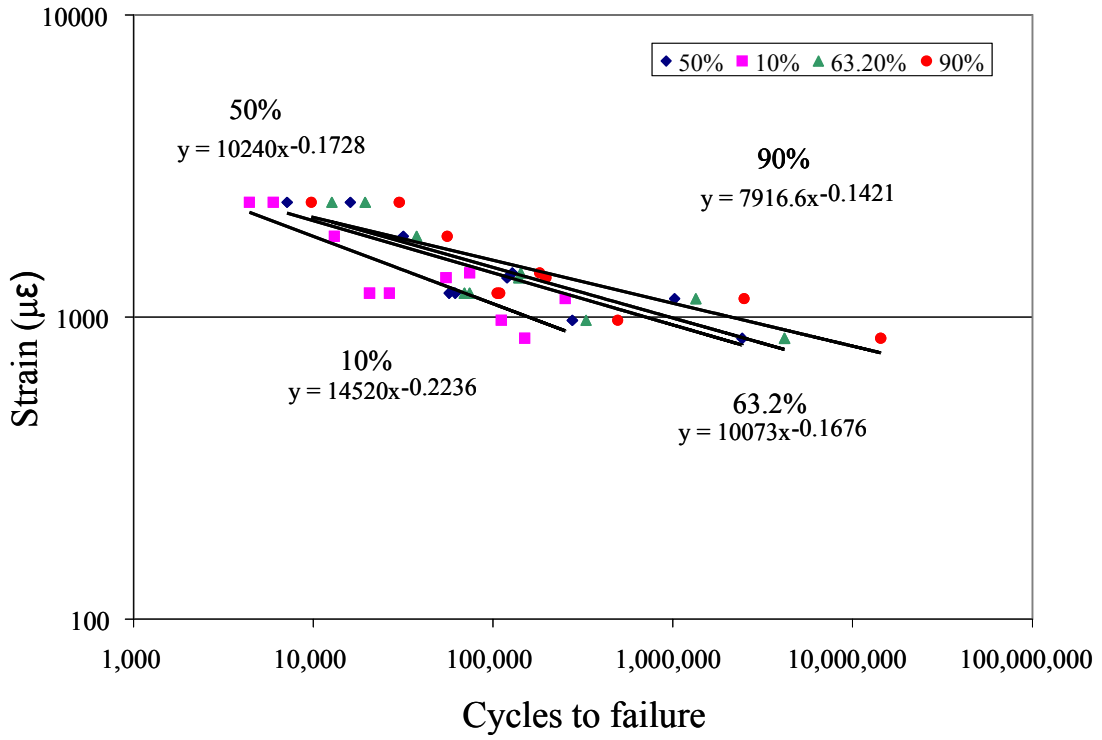


Figure 34. S-N curve with different failure probabilities

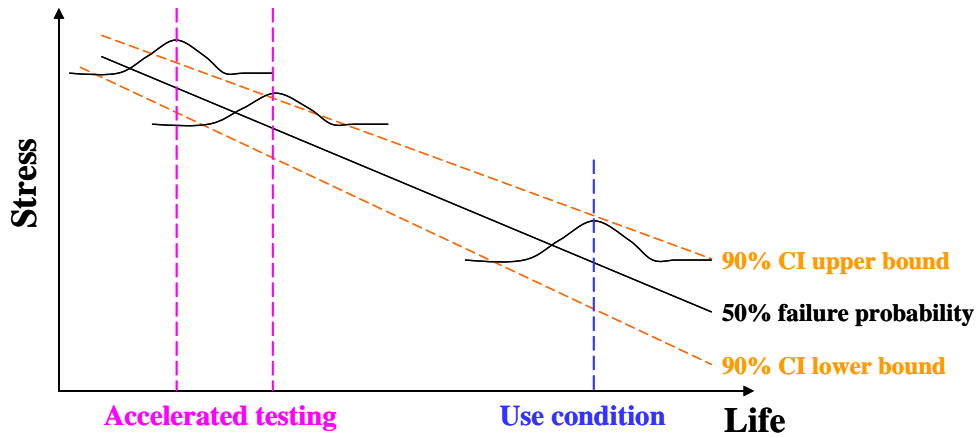


Figure 35. Confidence interval for S-N curve

5.2.4 Failure criteria uncertainty

From Miner's rule (Equation 5-3), the damage fraction (D) at any stress level is linearly proportional to the ratio of the number of cycles of operation (n_i) to the total number of cycles that would produce failure (N_i) at that stress level. When the summation of all the D (D_{total}) is larger than 1, the failure is considered to have occurred. However, safety margins may be taken into consideration in some situations. In addition, the loading sequences can affect the result [73]. So it is necessary to consider the failure criteria as an interval rather than one single data point. From the literature [73], the failure criteria value for D_{total} can change from 0.5 to 2.

$$D_{total} = \sum_{i=1}^n \frac{n_i}{N_i} \quad (5-3)$$

5.2.5 Future usage uncertainty

When uncertainty analysis is carried out, the assessment is based on the current and historical data points. In other words, the future usage is assumed to be the same loading level as the previous overall usage. However, in reality, the future usage profile or mission may vary from the previous one. It may be much more critical than the previous one, or the product will not be used for a while. The changes for usage loading condition were also mentioned in Chapter 3. All these types of situations will affect the prediction results. Details will be explained in the later paragraph.

5.3 Sensitivity analysis

Sensitivity analysis was conducted for the parameters listed above. The parameters were examined to see how they changed in real life. This accounts for considering the natural variability of the parameter, instead of the arbitrary selected criteria of say +/- 1%. Some parameters may change more, while others change less. For example, some parameters (PCB thickness, BGA span, solder ball pitch, solder ball height and solder ball diameter) can change due to the manufacturing process. Their variation range can be found from the manufacturer datebook and catalog [74][75][76][77][78]. These kinds of parameters were considered as normal distributions in this study. In the meantime, solder ball Young's modulus is a temperature dependent parameter, changing due to the environment and operational system, so a uniform distribution was assigned to represent a temperature range. Fatigue model constant, bin width effect and strain measure inaccuracy were also assigned uniform distributions. Percentage changes of damage accumulation for one hour due to the whole tolerance range of input parameters were calculated and shown in Table 12. Finally, the dimensionless nominal sensitivity index is found by normalizing the results (Equation 5-4) with the sensitivity index of all parameters considered. This enables the more accurate identification of the dominant parameters that influence the output of the damage model. Based on the sensitivity analysis the parameters that results in the maximum variation in the time to failure can be selected for the uncertainty propagation analysis.

$$\hat{S}_i = \frac{S_i}{\sqrt{\sum S_i^2}} \quad (5-4)$$

Table 12. Sensitivity analysis for uncertainty parameters

Input parameters (x_i)	Mean	Tolerance /Range	Percentage change (S_i) of one hour damage accumulation due to whole range	Normalized sensitivity index	Rank
BGA span	31.75 (mm)	+/- 0.25	16.8%	0.026	8
PCB thickness	1.829 (mm)	+/- 0.15	39.6%	0.061	4
Solder ball pitch	1.27 (mm)	+/- 0.04	21.8%	0.034	7
Solder ball height	0.52 (mm)	+/- 0.05	44.4%	0.069	3
Solder ball diameter	0.76 (mm)	+/- 0.05	57.0%	0.088	2
Solder ball Young's modulus	29914 (MPa) (303K)	25354 (333K) 34474 (273K)	22.4%	0.035	6
Fatigue constant – b	6.4	3.9 – 10.1	639.5%	0.989	1
Data binning width	Optimal	+/- 5.0%	2.6%	0.004	10
Combined trigger signal	NA	+ 3.7%	28.4%	0.044	5
Strain measurement	NA	+/- 3.98%	11.2%	0.017	9

In order to measure the uncertainty quantitatively, the uncertainty range is defined as the distance between the 1 and 99 percent point in the uncertainty distribution (Figure 36 gives the schematic explanation). It represents the precision of the predicted results. Then, all uncertainty sources can be checked to determine which parameter(s) or step(s) contribute most to the final uncertainty.

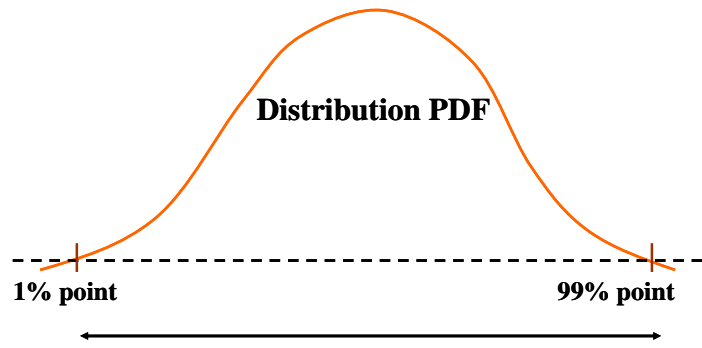


Figure 36. Uncertainty range

The damage uncertainty range is the uncertainty range for damage distribution. Figure 37 shows the first hour damage uncertainty range caused by variation of each parameter. In the calculation process, when an individual parameter was considered, such as the PCB thickness, it was considered as an input distribution, while other parameters were given a single fix value. The length of the individual bar in the figure is the damage uncertainty range for certain parameter, and the solid diamond is the mean value. The straight line represents the predicted damage without considering the uncertainty calculations. In many cases, the mean value would be near that straight line. In this analysis, the solder ball diameter and solder ball height were considered as coupled parameters, so the analysis was performed at the same time. This was also the case for the solder ball pitch and BGA span.

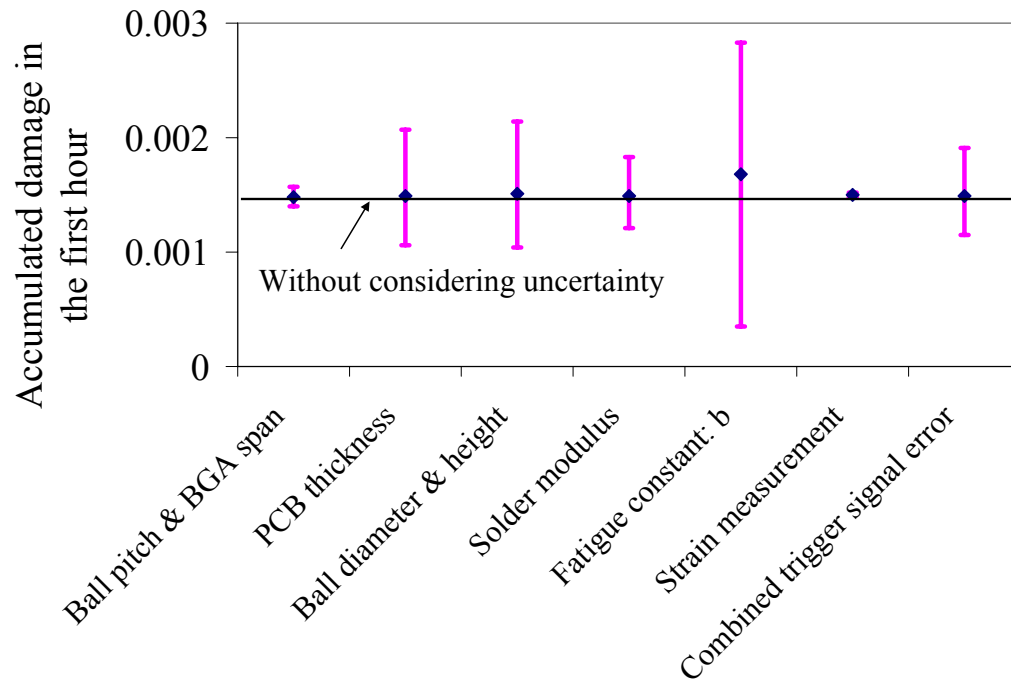


Figure 37. Damage uncertainty range for the first hour

The damage uncertainty range was also calculated for each parameter from Figure 37 and summarized in Table 13. The second column in the table was the damage range for each parameter. The third column gave the rank for these parameters. The fatigue constant was found to be the most critical parameter in this analysis. In real life, the fatigue constant will contribute even more. Since the damage range caused by the fatigue constant variation will be magnified by the acceleration factor when considering the real life loading condition compared to this accelerated test condition. Therefore, to reduce the uncertainty, the failure fatigue model must first be improved to get a more accurate material fatigue constant. The other observation from Table 13 is that the rank for the damage uncertainty range is similar

to the sensitivity analysis rank. Therefore, it is reasonable to assume that the first five parameters from the sensitivity analysis should be used to perform the uncertainty analysis, since they contribute the most to the final uncertainties.

Table 13. Damage uncertainty range for the first hour

Parameters	Damage uncertainty range	Rank
Ball pitch & BGA span	0.00017	6
PCB thickness	0.00101	3
Ball diameter & height	0.0011	2
Solder modulus	0.00062	5
Fatigue constant: b	0.00248	1
Strain measurement	4E-05	7
Combined trigger signal error	0.00076	4

5.4 *Uncertainty propagation*

The uncertainty propagation during the whole prediction process is shown in Figure 38. It shows the how the uncertainty propagates during the prognostics approach.

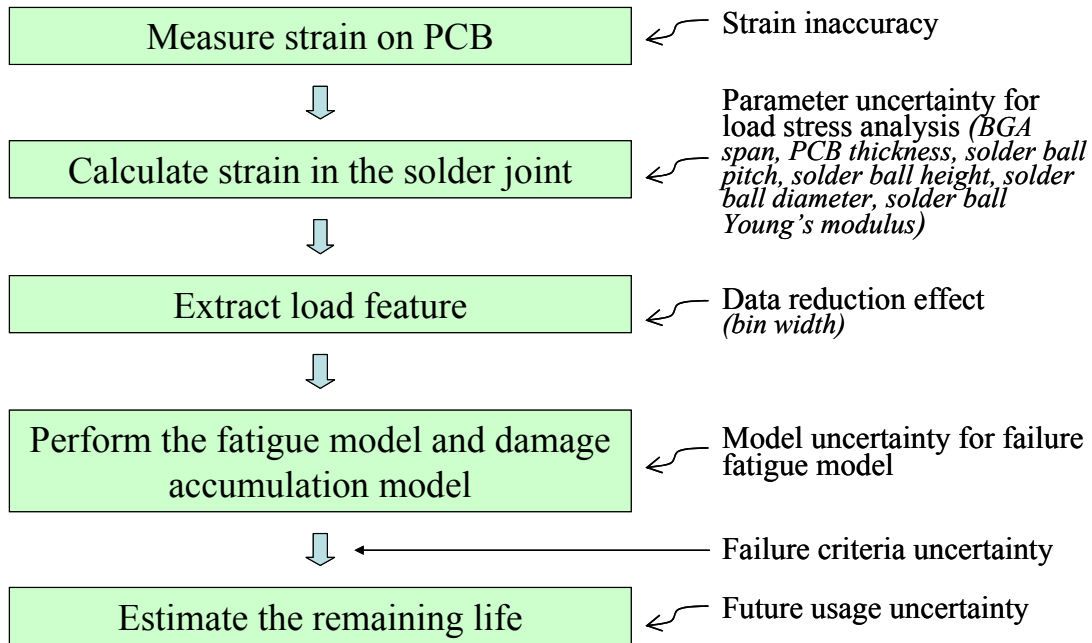


Figure 38. Uncertainty propagation

Traditional approach to calculate the uncertainty propagation is based on first order approximates shown as follows:

Let

$$Y = g(X) \tag{5-5}$$

For single random variable, mean value and variances can be calculated by,

$$\mu(Y) \approx g(\mu(X)) \tag{5-6}$$

$$\sigma_Y^2 \approx \left(\frac{dg(X)}{dX} \right)^2 \sigma_X^2 \tag{5-7}$$

where μ is mean value and σ is standard deviation. For multiple random variables, mean value can be calculated by,

$$\mu(Y) \approx g(\mu(X_1), \mu(X_2), \dots, \mu(X_n)) \quad (5-8)$$

And variances can be calculated by Equation (5-7) if variables are correlated with each other,

$$\sigma_Y^2 \approx \sum_{i=1}^n \sum_{j=1}^n \frac{\partial g(X)}{\partial X_i} \frac{\partial g(X)}{\partial X_j} Cov(X_i, X_j) \quad (5-9)$$

If variables are not correlated with each other, variances can be calculated by,

$$\sigma_Y^2 \approx \sum_{i=1}^n \left(\frac{\partial g(X)}{\partial X_i} \right)^2 \sigma_X^2 \quad (5-10)$$

The disadvantage of above analytical approach is that the first order approximation will not be accurate when the equation is nonlinear. Therefore in this research, the Monte Carlo simulation was used. The steps for using the Monte Carlo simulation [79] are as follows: first, generation random numbers; second, generation of random variables using transformation methods from random numbers; third, evaluation of the model multiple times (m simulation cycles); last, statistical analysis of the resulting behavior. More detailed steps are given in Appendix C.

The overall approach to implement Monte Carlo simulation into uncertainty is shown in Figure 39. This approach utilizes a sensitivity analysis to identify the dominant input variables that influence the model-output. With information of input parameter variable distributions, a Monte Carlo simulation is used to provide a distribution of accumulated damage. From that, the remaining life is then predicted

with confidence intervals. In addition, the failure criteria and future usage uncertainty will be considered when performing the remaining life assessment.

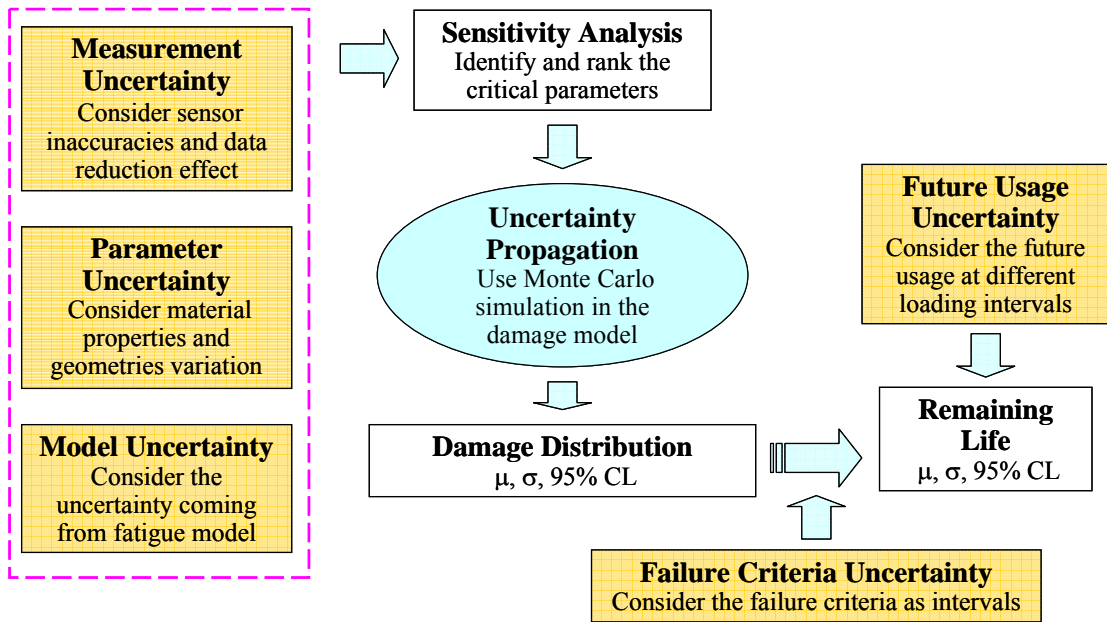


Figure 39. Uncertainty analysis procedure for prognostics

Based on the updated rank in Table 12, the first five parameters' uncertainties were considered critical, thus they were selected to assess the uncertainty of the remaining life prediction. The solder ball diameter and height are dependent on each other. When two parameters are coupled, the following steps can be used to generate the distributions: first, let the two distributions that are correlated be $f(x)$ and $f(y)$; then calculate the correlation coefficient, ρ , from Equations (5-11) through (5-15); after that, random sample for $f(x)$ distribution N times to get $X = \{x_1, x_2, \dots, x_N\}$; then

calculate y_i for each value of x_i based on ρ and variance in x and y using Equation (5-15); last, use new pairs of (x_i, y_i) together in the Monte Carlo simulation.

$$\rho = \frac{\text{cov}(x, y)}{S_x S_y} \quad (5-11)$$

$$\text{cov}(x, y) = \frac{\sum (x_i - \bar{x})(y_i - \bar{y})}{n-1} \quad (5-12)$$

$$S_x = \sqrt{\frac{\sum (x_i - \bar{x})^2}{n-1}} \quad (5-13)$$

$$S_y = \sqrt{\frac{\sum (y_i - \bar{y})^2}{n-1}} \quad (5-14)$$

$$\hat{y} = \frac{\rho S_y}{S_x} (x - \bar{x}) + \bar{y} \quad (5-15)$$

where S_x and S_y are the variance of $f(x)$ and $f(y)$.

In this study, the solder volume, V , was fixed. The solder ball height (h) was calculated using Equation (5-16) from the solder ball diameter (D) when the solder volume was known. However, solder volume was also a variable; therefore a distribution was also assigned for the volume. That is to say, the first two independent distributions were generated: one for solder ball diameter and the other for solder ball volume. Then the solder ball height was calculated using random numbers from those two distributions. Finally, the solder ball diameter and solder ball height were used in the Monte Carlo simulations.

$$V = f(D, h) \quad (5-16)$$

The five most critical parameters (PCB thickness, solder ball diameter, solder ball height, failure fatigue constant, and data reduction error) were selected for uncertainty analysis. The probability density function (PDF) was assigned for each

parameter as shown in Figure 40. These distributions were input into a Monte Carlo simulation. In Figure 40, the mean value of accumulated damage in one hour became stable when the Monte Carlo sample size was increased, and Equation (5-17) was used to control the simulation sample size.

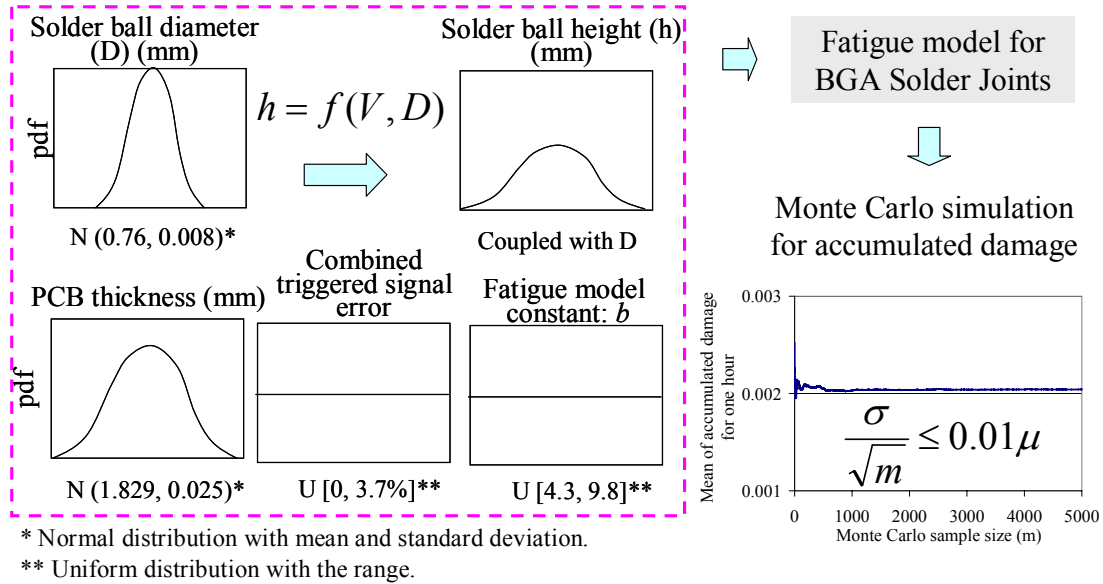


Figure 40. Input parameters for Monte Carlo simulation

Figure 41 shows the distribution of the accumulated damage in the first hour. Lognormal is the most suitable distribution to fit the data in this case. The mean value of the distribution is 0.00204, and the upper and lower limit bound was calculated for a 95 percent confidence level. A similar distribution was obtained for each hour that followed. The total damage distribution was calculated by adding together the damage distributions for each previous hour, as shown in Figure 42. When the damage accumulates with time, the uncertainty also accumulates with time. Five different failure probability curves shown in Figure 43 were used to present how the

damage and uncertainty accumulated: 1 percent, 5 percent, 95 percent, 99 percent and mean time to failure (MTTF). The uncertainty becomes wider as the time increases.

One percent probability implies much faster failure than 99 percent.

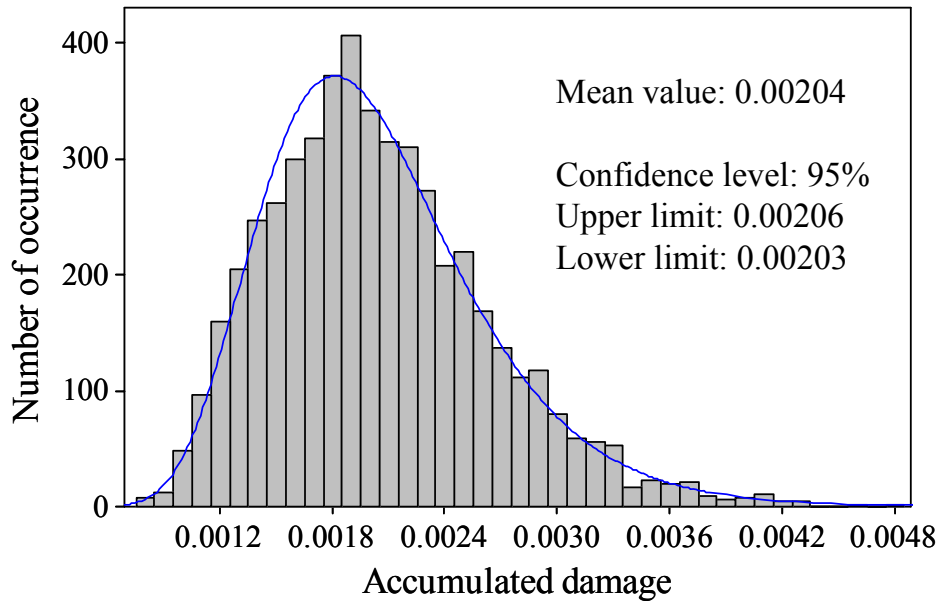


Figure 41. Accumulated damage distribution for one hour

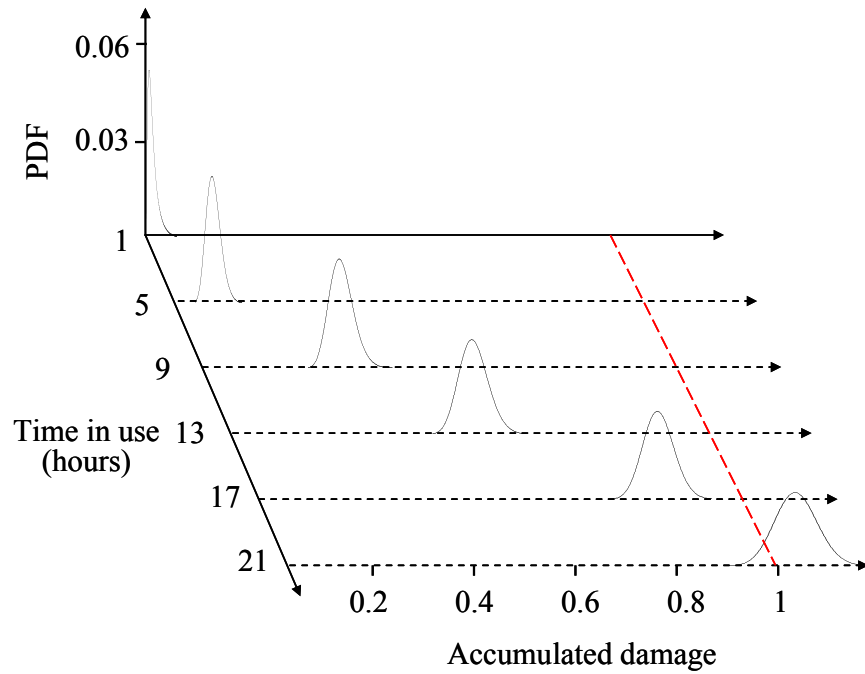


Figure 42. Uncertainty propagation with damage accumulation

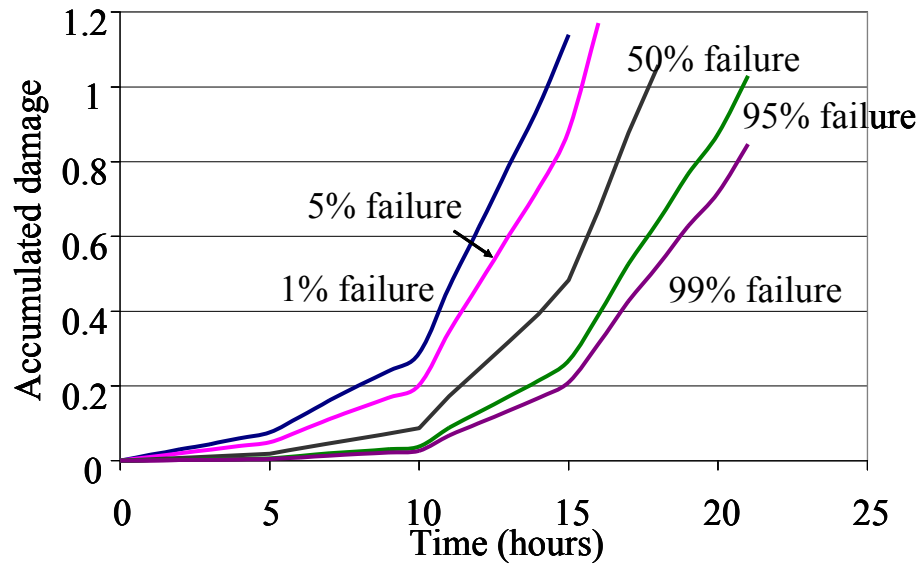


Figure 43. Damage accumulation with time at different failure probabilities

Figure 44 shows the remaining life prediction based on the different failure probabilities. The actual failure point is between 50 and 95 percent of the failure

probability. The accuracy of the prediction results compared to the experimental results is 3 hours, which is calculated from the difference between 50% failure probability prediction result and actual experiment failure time. The precision of prediction result is 10.5 hours, which is calculated from remaining life uncertainty range (the distance between 1% point and 99% point of distribution).

It was also shown in Figure 44 that remaining life estimates become more precise as the time to failure decrease since real loading condition was recorded and used in the prediction procedure. In the first hour, the predicted remaining life uncertainty range is 978 hours; while in the fourteenth hour, it is only 68 hours.

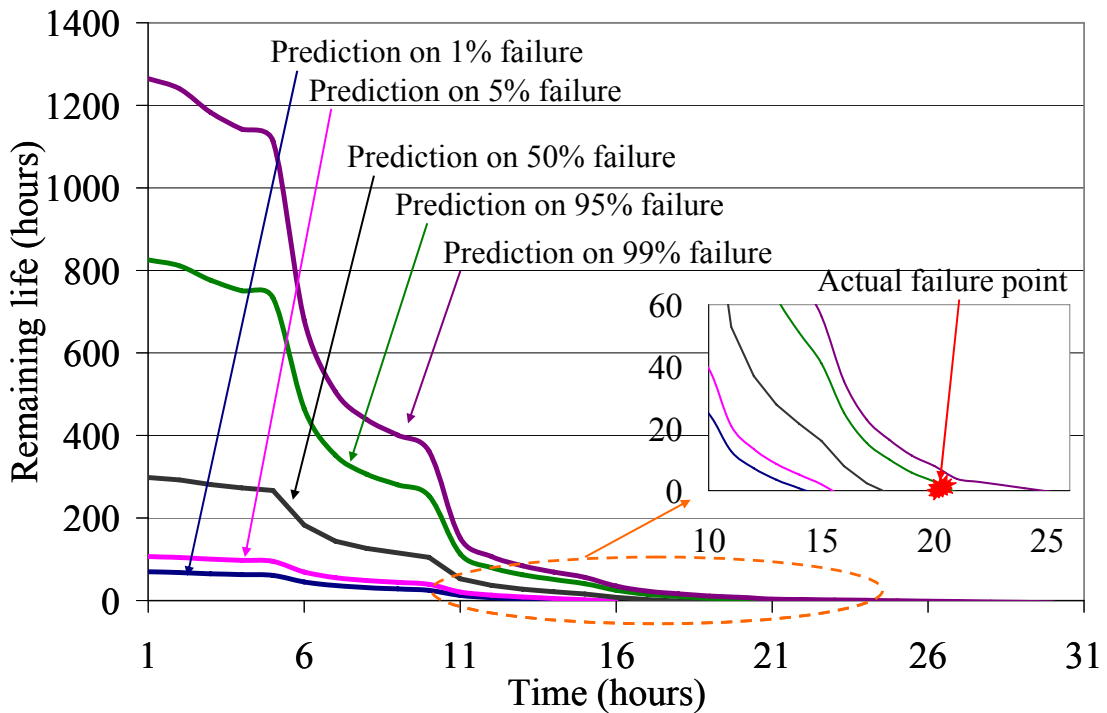


Figure 44. Remaining life prediction at different failure probabilities

5.5 Prediction Considering Failure Criteria Uncertainty

Failure criteria will be affected by the loading sequence and safety concerns. If the application involves human participation (such as aircraft or spacecraft) or may compromise the safety of personnel (such as machinery in a factory), a lower limit of damage accumulation may be chosen, but if the application is known to be fairly reliable (such as for systems with multiple redundancy), a higher limit of damage accumulation may be selected.

In the previous section, it is mentioned that the failure criteria (accumulated damage to failure) can vary from 0.5 to 2. The traditional approach to calculate the reliability can refer to Equation (5-20) and Figure 45.

$$R = P(D_{total} < C / 0.5 < C < 2) = \int_0^{\infty} f_D(D) \left[\int_D^{\infty} f_c(C) dC \right] dD \quad (5-20)$$

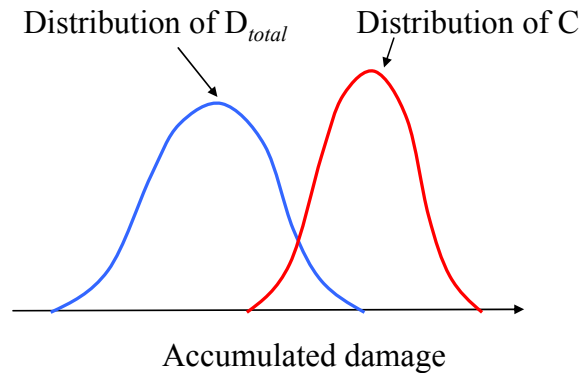


Figure 45. Conditional reliability estimation

where D is the distribution of accumulated damage, and C is the distribution of failure criteria. The disadvantage is that it can not show clearly how the change of failure criteria affects the remaining life prediction. For example, if the failure criteria uncertainty was changed, the calculation should be performed again.

In this study, interval analysis will be conducted. Three different levels (see Table 14) were considered because of different safety concerns. When a given level was selected for the application, the predicted remaining life bounds were calculated with failure probability. In this study, 5 percent failure probability was used; the prediction results were shown in Table 15 and Figure 46. The lower/upper bound in Table 15 was the bound for the input interval in Table 14. For example, when the failure criteria interval was from 0.5 to 1, the predicted life can be from 12.07 to 15.41 hours. When there was less concern for safety, predicted remaining life can increase. The different failure criteria would not only affect the final prediction point, they would also affect the prediction from the beginning, as shown in Figure 46.

Table 14. Failure criteria uncertainty categorization

Safety concern	High	Normal	Low
Accumulated damage to failure	0.5 – 1.0	1.0 – 1.5	1.5 – 2.0

Table 15. Remaining life prediction considering failure criteria uncertainty

Safety issue	Remaining life prediction (hours) on 5% probability failure	
	Lower bound	Upper bound
High	12.07	15.41
Normal	15.41	17.13
Low	17.13	18.76

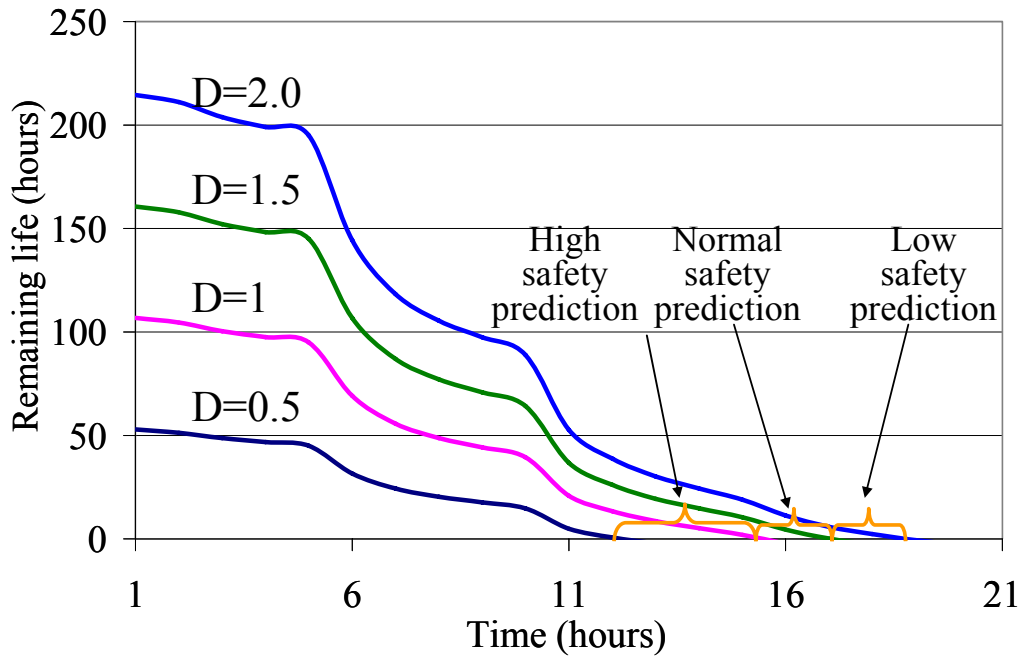


Figure 46. Remaining life prediction considering failure criteria uncertainty

5.6 Prediction Considering Future Usage Uncertainty

Normally the prediction of reliability (remaining life) is based on the overall damage from the current and historical data and trends. If the future usage data is different from the historical usage profile, then the prediction will become inaccurate. Therefore, it is necessary to consider the variability of the future usage profiles. In addition, the remaining life assessment in different loading conditions can help users

in making decisions, such as whether the product can still be used in low loading conditions for a couple of hours but not in high loading conditions.

One method for counting usage loading uncertainty is to categorize the usage loading based on the distribution of accumulated damage. As shown in Figure 47, from damage distribution, it is easy to categorize different damage levels which are related to different loading levels. For example, high damage means high loading conditions. Then the remaining life prediction can be estimated based on the high loading, which uses the damage data at the right part of the distribution. The advantage of this approach is that it is easy to use and implement into prognostics. The disadvantage is that it is limited to the history loading conditions. In other words, if the loading is never happen before, then it is impossible to know the damage distribution.

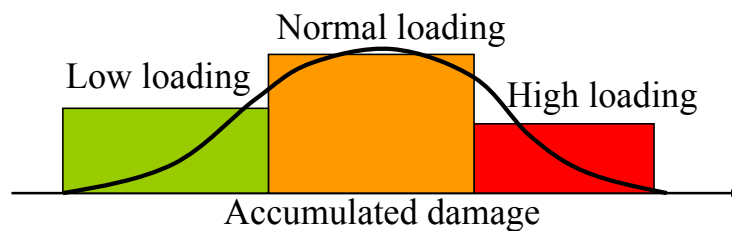


Figure 47. Future loading categorizations from accumulated damage

In this study, usage loading intervals analysis is used, which is similar approach to the failure criteria uncertainty calculation. Since it is known that there are four loading levels and the tests are step stress increasing loading. Therefore, even if one counts the high loading part in Figure 47, which is the highest loading condition in the past, it is still less than the future loading. That is the reason interval analysis is being used. In this demonstration case three levels were considered: a low loading condition, a normal loading condition, and a high loading condition, with corresponding input PSD levels (see Table 16). A prediction was made at the tenth hour based on different usage levels, as shown in Table 17. The lower/upper bound of remaining life corresponds to the input PSD intervals. For example, in the normal loading condition (PSD from 0.1 to 0.3 G²/Hz); the predicted remaining life is from 2.22 to 26.21 hours. The “0” in Table 17 occurs if there is sudden shock loading, while “infinite” means the product is not in use. Figure 48 shows how future usage loading data can affect the prediction results. This analysis can help evaluate whether the product is suitable for the next mission or for a couple of times. Of course, since the loading conditions may change, in situ monitoring and prediction is preferred and can give more accurate results.

Table 16. Future usage loading level categorization

Future usage	Low loading	Normal loading	High loading
Input PSD level (G ² /Hz)	0 – 0.1	0.1 – 0.3	> 0.3

Table 17. Remaining life prediction considering future usage uncertainty

Future usage profile	Remaining life prediction (hours) of 5% probability failure at the 10 th hour	
	Lower bound	Upper bound
Low loading	26.21	Infinite
Normal loading	2.22	26.21
High loading	0	2.22

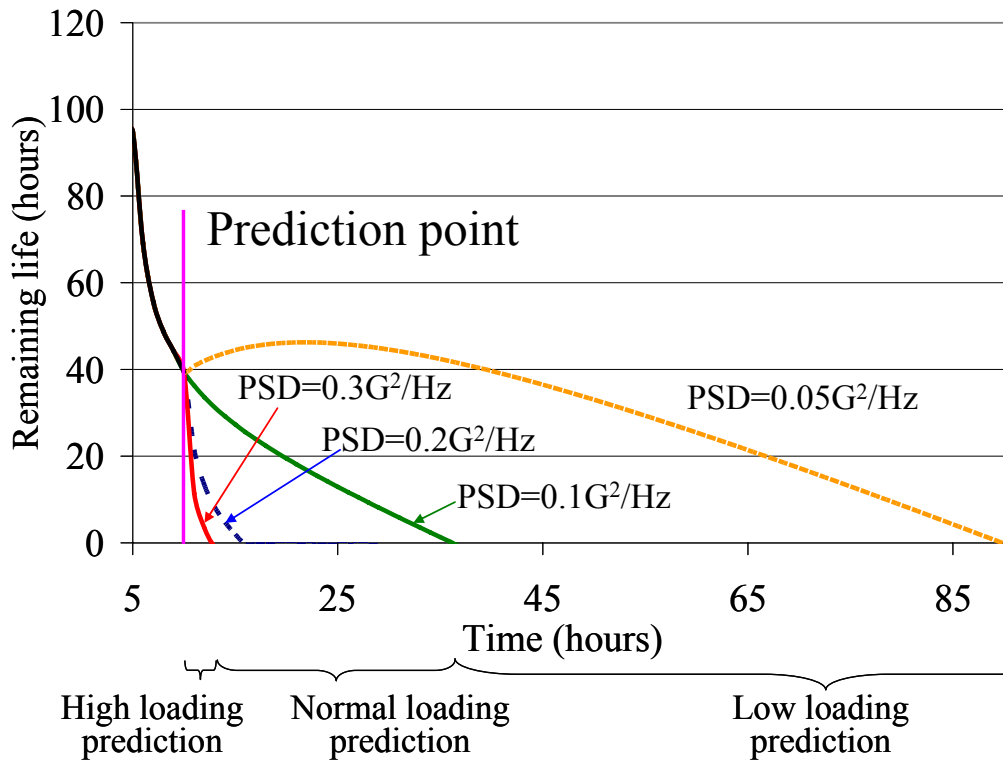


Figure 48. Remaining life prediction considering future usage uncertainty

From Figure 48, we noticed that the remaining life increased for the low loading prediction. It caused confusion many times. If there is a wide variation in system usage, increment in the remaining life may occur based on the calculation from Equation (4-34). In order to overcome this confusion, Equation (5-21) was provided. By using new equation, the remaining life always shows the decreasing

trend. However, the disadvantage for new equation is that the accuracy of the prediction is dominated by the initial prediction, since the rest prediction results will be smaller than this value. If the initial usage loading is much higher than the normal usage condition, the prediction will be misleading.

$$RL_N = RL_{N-1} - D_N * TL_{N-1} \quad (5-21)$$

where RL_N is the remaining life at the end of N hours, RL_{N-1} is the remaining life at the end of N-1 hours, D_N is the accumulated damage at the Nth hour, and TL_{N-1} is the total life predicted at (N-1)th hour.

Therefore Equation (4-34) is used for the remaining life prediction when the future loading condition is unknown. In the case of Figure 48, it was used for first 10 hours predictions. Equation (5-21) is used for the remaining life prediction when the future loading condition is known. In the case of Figure 48, it was used after first 10 hours predictions. The updated prediction result was shown in Figure 49. It was found out that if there was no loading, the remaining life would remain the same, which means no life was consumed.

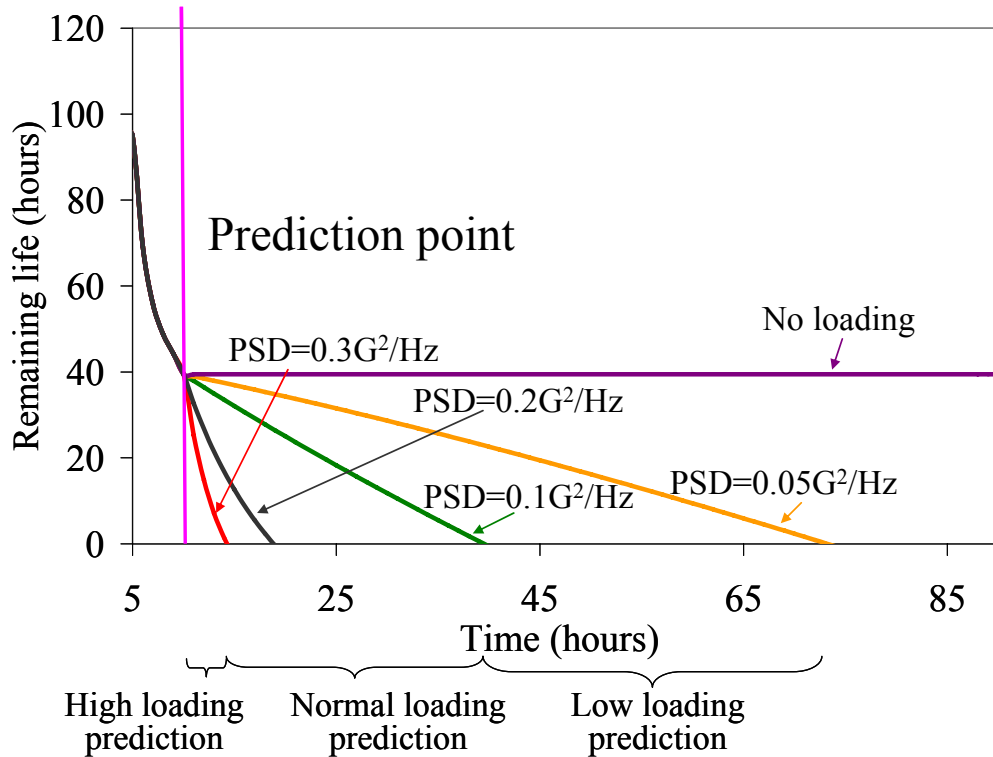


Figure 49. Updated remaining life prediction considering future usage uncertainty

5.7 Summary

In this chapter, an approach for applying uncertainty analysis to PoF-based prognostics has been provided. The approach utilizes sensitivity analysis to identify the dominant input variables that influence model output. The approach also uses the distributions of input variables in a Monte Carlo simulation to provide a distribution of accumulated damage. Given the measurements, parameters, model, failure criteria, and future usage uncertainty, the actual failures in testing were observed to occur within the predicted failure distribution. The sensitivity analysis procedure revealed that it is important to consider the tolerances of the parameter variables, as they can strongly influence the ranking of the most sensitive variables. It was also determined

that the fatigue constant is a key contributor to uncertainty. Based on the uncertainty assessment, the prognostic approach enables the user to make remaining life predictions with fewer data sets, and initial rough estimates can be made before all of the model parameters are collected or any future loading is recorded. These estimates are valuable for initial planning. When sufficient usage data and model parameters are available, the estimates will provide more accurate predictions that enhance decision making. It was observed that the prediction accuracy increased with a decrease in the remaining life of the product. This was attributed to the fact that with increased usage there was more data to support the prognostics.

Chapter 6: Contributions and future work

This thesis has developed a time domain prognostics approach for solder joint reliability under vibration loading using in-situ random strain/acceleration data. This approach integrates data collection, strain transformation, damage assessment, and remaining life calculation technology. Related work includes the development and verification of a space-saving approach for in-situ vibration data storage and development of an approach for the remaining life prediction of multiple components using a single sensor based on mode shape analysis to enhance prognostics capability.

This thesis also presented an approach to assess the uncertainties for remaining life prediction of solder joints under vibration loading. The approach includes uncertainty source identification, sensitivity analysis, and uncertainty propagation. The work provides quantitative insights into the sensitivity of remaining life prediction based on different uncertainty sources. Identification of model uncertainty is critical for remaining life prediction. This is the first study to evaluate model uncertainty based on accelerated testing and S-N curve data. It is the first study to predict remaining life based on different failure criteria using intervals, which enables the safety factor to be an input. And it is the first study to predict remaining life based on future usage conditions, which are estimated from current and historic loads by utilizing the damage distributions.

Future work can include:

(1) Investigation of the integration of self-partition technology (the partition between the time trigger and the signal trigger) into in-situ vibration data recording. The frequency of the time trigger and the optimal threshold for the signal trigger can be studied to improve the accuracy of combined trigger signal recording. The technology for accuracy verification of the combined trigger signal and the continual monitoring signal can also be improved using the non-linear superposition approach.

(2) Investigation of high mode frequency and mode superposition for other possible kinds of vibration loading, since in real life the first mode of vibration is not always dominant.

(3) Implementation of a sensor network (strain gauge and accelerometer) to enhance prognostics accuracy. In real life, the sensors may not be as reliable as the monitored product. If a sensor fails earlier than the product, it will lose its capability for prognostics and even give a false alarm. A sensor network can monitor the health of a sensor for better accuracy. In addition, prognostics decisions can be made from the results of multiple sensors instead of only one, which will enhance accuracy.

(4) Consideration of other uncertainty sources those were not included in this thesis. For example, uncertainty will come from the strain transfer function between a quasi-static (not considering inertial force) and a dynamic model (considering inertial force), FEA mesh size, the FEA strain/stress average approach, and so on.

Appendix A: Combined Loading Calculation

In many cases, it is impossible to conduct continual recording, therefore combined loading recording should be used. It combines the time triggered and signal triggered recording technology.

For example, in one simple vibration loading record study, the sample frequency is 1024Hz, and it is recorded for 180s. In the time triggered situation, we do not record the whole 180 seconds, and we are recording every 30 seconds. That is to say: 1st second, 31st second, 61st second, 91st second, 121st second, 151st second, and totally they are 6 seconds (3.33% of original data points), as shown in Figure 50. Those 6 seconds will represent for whole 180 seconds. Therefore the histogram of time triggered recording in Figure 24 will time 30 (180/6). The purpose for time triggered recording is to captures the general distribution of the loading.

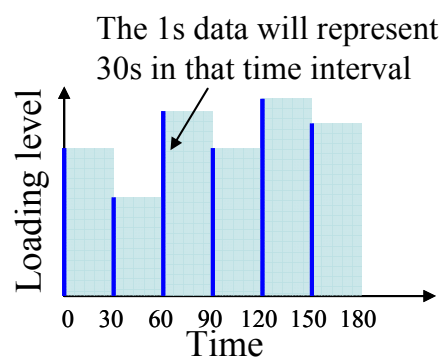


Figure 50. Time triggered recording

In the signal triggered situation, we also do not record the whole 180 seconds, and we are recording when the signal is above pre-set threshold. In this case, it records 3 separated seconds (1.67% of original data points), as shown in Figure 51. Those 3 seconds will represent for whole 180 seconds. Therefore the histogram of signal triggered recording in Figure 24 will time 60 (180/3). The purpose for signal triggered recording is to capture the abnormal stress conditions, such as shock, during a gap in the time trigger function.

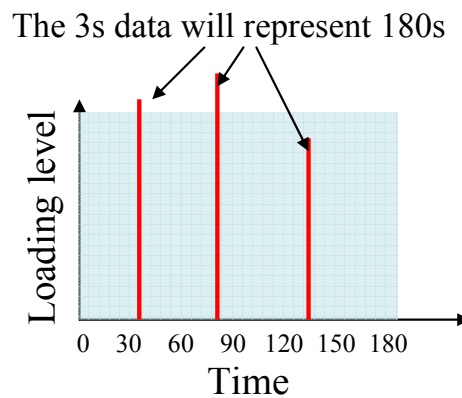


Figure 51. Signal triggered recording

For the combined trigger recording situation, it totally has 9 events (5% of original data points, 6 from time trigger and 3 from signal trigger). It can be calculated using Equation (A-1):

$$Y3 = Y1 * (180 - 3) / 180 + Y2 / 60 \quad (A-1)$$

where Y1 is the Y axis for the time trigger recording in Figure 24, Y2 is the Y axis for the signal trigger recording in Figure 24, and Y3 is the Y axis for the combined trigger recording in Figure 24.

Appendix B: Cycle Counting

Cycle counting methods [80] are used to transform a time history consisting of several reversals (peaks and valleys) into an equivalent cyclic history. Cycle counting methods are used when a fatigue analysis needs to be performed.

The physical interpretation of a cycle is a condition when the applied load returns the material to the state it was before the load excursion occurred. If the applied load is of a mechanical nature (such as force or torque), the material forms a closed stress-strain hysteresis loop when this condition is satisfied. For a repeatedly applied load history, the following two rules apply [81]:

- When the load reaches a value at which loading was previously in the reverse direction, a stress-strain hysteresis loop is closed, defining a cycle. The stress-strain path beyond this point is the same as if the loading had not been reversed.
- Once a load sequence forms a closed loop, this sequence does not affect the subsequent behavior.

For the load history shown in Figure 52 [81], the first rule is invoked at points 2', 7', 5', and 1'. The first rule is also satisfied just beyond 5', where the load reaches the same value it had at point 3. But the second rule also applies, and since excursion 2-3-2' has already formed a cycle, there is no additional closed cycle.

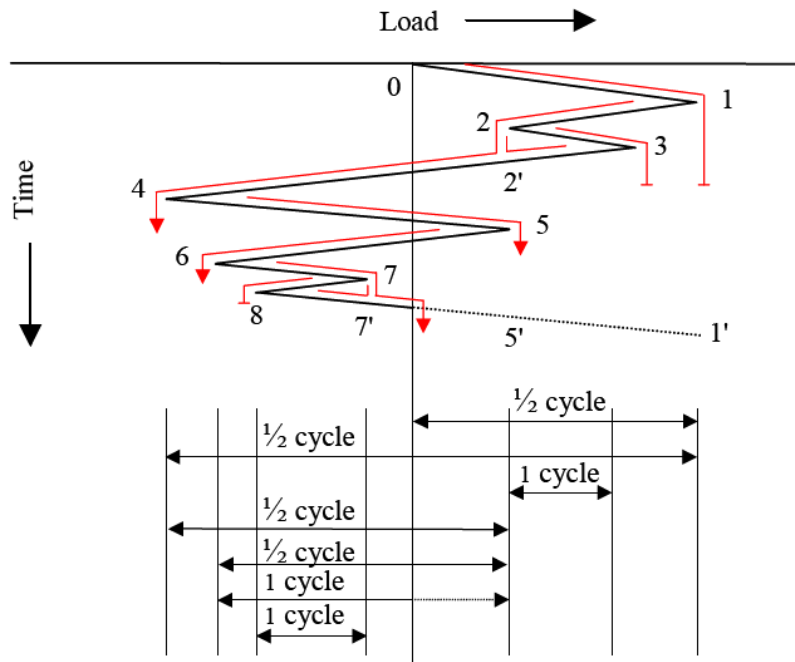


Figure 52. Cycle identification

For non-repeating and open-ended load histories, the rules stated above are incomplete if the absolute value of the load at any point during the history exceeds its value at the first peak. Of the various cycle counting methods available (peak counting, simple range counting, peak-between mean counting, level crossing counting, fatigue meter counting, range-pair counting, and rainflow counting), only the rainflow and the range-pair counting methods are capable of handling this more general situation (of non-repeating histories).

In the rainflow cycle counting method, the load-time history is plotted in such a way that the time axis is vertically downward, and the lines connecting the load peaks are imagined to be a series of sloping roofs. The rain flow is initiated by placing drops successively at the inside of each reversal. The method considers cycles as closed hysteresis loops formed during a history, which is consistent with the definition of a cycle described in the previous section. Following rules are applied on the rain dripping down the roofs to identify cycles and half cycles:

- The rain is allowed to flow on the roof and drip down to the next slope except that, if it initiates at a valley, it must be terminated when it comes opposite a valley equal to or more negative than the valley from which it initiated. For example, in Figure 53 [81], the flow begins at valley 1 and stops opposite valley 9, valley 9 being more negative than valley 1. A half cycle is thus defined between valley 1 and peak 8.

- Similarly, if the rain flow is initiated at a peak, it must be terminated when it comes opposite a peak equal to or more positive than the peak from which it initiated. In Figure 53, the flow begins from peak 2 and stops opposite peak 4, peak 4 being more positive than peak 2. A half cycle is thus counted between peak 2 and valley 3.

- The rain flow must also stop if it meets rain from a roof above. Figure 53, the flow beginning at valley 3 ends beneath peak 2. This ensures that every part of the load history is counted once and only once.

- Cycles are counted when a counted range can be paired with a subsequent range of equal magnitude in the opposite direction. If cycles are to be counted over the duration of a profile that is to be repeated block by block, cycle counting should be started by initiating the first raindrop either at the most negative valley or at the most positive peak, and continuing until all cycles in one block are counted in sequence. This ensures that a complete cycle will be counted between the most positive peak and the most negative valley.

The simple rainflow method does not provide any information about the mean load or the cycle time. A modified method called 3-parameter rainflow cycle counting is used to handle this situation. This method accepts a sequence of successive differences between peak and valley values (P/V ranges) in the time history as an input, and determines the range of the cycle, the mean of the cycle, and the cycle time.

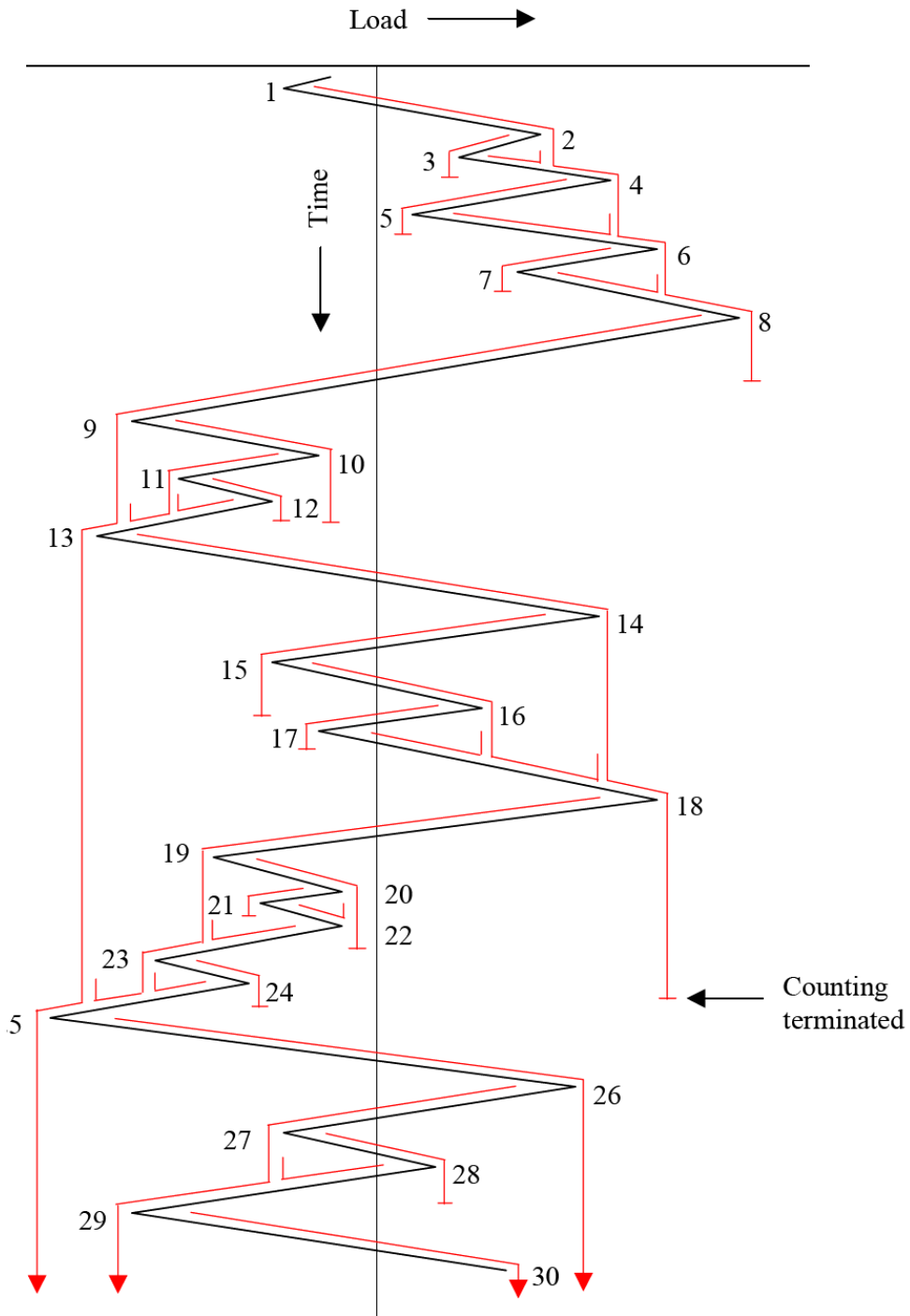


Figure 53. Rainflow cycle counting

Appendix C: Monte Carlo Simulation

In random sampling, variates are generated using the inverse cumulative function. Let $f(x)$ is the power density function (PDF) with $0 < x < \infty$ and $F(x)$ is the cumulative density function (CDF) of random variable x .

To generate the random variates, we first define R a random variable uniformly distributed over $[0, 1]$. Then the inverse CDF is given by;

$$x = F^{-1}(R) \tag{C-1}$$

For multiple variable, by using same method, we can get series variates as x_1, x_2, \dots, x_m . Then we can evaluate the y by using Equation B-2 and store the results as y_j .

$$y = f(x_1, x_2, \dots, x_n) \tag{C-2}$$

where m is the number of variates.

Repeat above steps, and get a series of y from different combination of x_i , then analyze the results using statistics and give the confidence levels for estimated y . Normally the higher the confidence levels, the more loops need to repeat to calculate the y . The stopping criterion for the Monte Carlo simulation is based on minimizing

the variance over the mean of the simulation results. For example, if, y_1, y_2, \dots, y_m are the results of the simulation, then the simulation stopped when:

$$\frac{\sigma}{\sqrt{m}} \leq 0.01\mu \quad (\text{C-3})$$

Here, the mean and variance are calculated as follows:

$$\mu = \frac{1}{m} \sum_{i=1}^m y_i \quad (\text{C-4})$$

$$\sigma^2 = \frac{1}{m-1} \sum_{i=1}^m (y_i - \mu)^2 \quad (\text{C-5})$$

Case study for Monte Carlo simulation can be found at reference [79].

References

- [1]. Pecht, M.; "Why the Traditional Prediction Molders Do Not Work – Is There an Alternative?" *Electronics Cooling*, 1996, Vol. 2, No. 1.
- [2]. Pecht, M.; and Nash, F.; "Predicting the Reliability of Electronic Equipment," *Proceedings of the IEEE*, 1994, Vol. 82, No. 7, pp. 992-1004.
- [3]. Cushing, M.J.; Mortin, D.E.; Stadterman, T.J.; and Malhotra, A.; "Comparison of Electronics-Reliability Assessment Approaches," *IEEE Transactions on Reliability*, 1993, Vol. 42, No. 4, pp. 542-546.
- [4]. Jones, J.; and Hayes, J.; "A Comparison of Electronic-Reliability Prediction Models," *IEEE Transactions on Reliability*, 1999, Vol. 48, No. 2, pp. 127-134.
- [5]. Luthra, P.; "MIL-HDBK 217: What is Wrong with it?" *IEEE Transactions on Reliability*, 1990, Vol. 39, pp. 518.
- [6]. Pecht, M.; *Prognostics and Health Management of Electronics*, Wiley-Interscience, New York, NY, 2008.
- [7]. DoD 5000.2 Policy Document, *Defense Acquisition Guidebook*, Chapter 5.3 – Performance Based Logistics, December 2004.
- [8]. Lau, J.; "Solder Joint Reliability of Surface Mount Connectors," *Journal of Electronic Packaging*, Vol. 115, 1993, pp. 180-188.
- [9]. Lee, S.B.; and Ham, S.J.; "Experimental Study for Reliability of Electronic Packaging under Vibration," *Experimental Mechanics*, Vol. 36, No.4, 1996, pp. 339-344.
- [10]. Zhou, Y.; Scanff, E.; and Dasgupta, A.; "Vibration Durability Comparison of Sn37Pb vs SnAgCu Solders," 2006 ASME International Mechanical Engineering Congress and Exposition, Chicago, Illinois, November 5-10, 2006.
- [11]. Zhou, Y.; and Dasgupta A.; "Vibration Durability Assessment of Sn3.0Ag0.5Cu & Sn37Pb Solders under Harmonic Excitation," 2007 ASME International Mechanical Engineering Congress and Exposition, Seattle, Washington, November 11-17, 2007.
- [12]. Basaran, C.; Alexander, C.; Yang Z.; and Dishongs, T.; "Reliability of BGA Under Vibrations," *Proceeding Of the Surface Mount Technology International Conference*, September, 2001.

- [13]. Yang, Q.J.; Wang, Z.P.; Lim, G.H.; Pang, F.; and Lin, R.M.; "Reliability of PBGA Assemblies under out-of-plane Vibration Excitations," IEEE Transactions on Components and Packaging Technologies, Vol. 25, No.2, June, 2002, pp. 293-300.
- [14]. Wong, T.E.; Palmieri, F.W.; and Kachatorian, L.A., "Experimentally Validated Vibration Fatigue Life Prediction Model for Ball Grid Array Solder Joint," ASME Packaging of Electronic and Photonic Devices, Vol. 28, 2000, pp.113-118.
- [15]. Wong, T.E.; Palmieri, F.W.; Reed, B.A.; Fenger, H.S.; Cohen, H.M.; and Teshiba, K.T.; "Durability/Reliability of BGA Solder Joints under Vibration Environment," 50th Electronic Components & Technology Conference, Las Vegas, NV, May, 2000.
- [16]. Qi, H.; Osterman, M.; and Pecht, M.; "Design of Experiments for Board Level Solder Joint Reliability of PBGA Package under Various Manufacturing and Multiple Environmental Loading Conditions," IEEE Transactions on Electronics Packaging Manufacturing, 2007.
- [17]. Basquin, O. H., "The Exponential Law of Endurance Tests," ASTM Proceedings, Vol. 10, 1910, pp. 625-630.
- [18]. Steinberg, D.; Vibration Analysis for Electronic Equipment, third edition, John Wiley & Sons, Inc. 2000.
- [19]. Sidharth, D.B.; and Barker, D.B.; "Vibration Induced Fatigue Life Estimation of Corner Leads of Peripheral Leaded Components," Journal of Electronic Packaging, Vol. 118, 1996, pp.244-249.
- [20]. Pitarresi, J.M.; Celetka, D.; Coldwel, R.; and Smith, D.; "The Smearred Properties Approach to FE Vibration Modeling of Printed Circuit Cards," ASME Journal of Electronic Packaging, Vol. 113, 1991, pp. 250-257.
- [21]. Suhir, E.; "Could Compliant External Leads Reduce the Strength of a Surface Mounted Device?" proceedings of the 38th Electronic Components Conference, 1988, pp. 1-6.
- [22]. Barker, D.; Chen, Y.S.; and Dasgupta, A.; "Estimating the Vibration Fatigue Life of Quad Leaded Surface Mount Components," Journal of Electronic Packaging, Vol. 115, 1993, pp. 195-200.
- [23]. Engel, P.A.; "Structural Analysis for Circuit Card Systems Subject to Bending," ASME journal of Electronic Packaging, Vol. 112, 1990, pp. 2-10.

- [24]. Singal, R.K.; and Gorman, D.J.; "A General Analytical Solution for Free Vibration of Rectangular Plates on Fixed Supports and with Attached masses," ASME Journal of Electronic Packaging, Vol. 114, 1992, pp.239-425.
- [25]. Darbha, K.; Ling, S.; and Dasgupta, A.; "Stress Analysis of surface Mount Interconnects Due to Vibration Loading," Proceedings of the 1996 ASME international Mechanical Engineering Congress and Exhibition, 1996, pp. 1-14.
- [26]. Roberts, J.C.; and Stillo, D.M.; "Random Vibration Analysis of a Printed Wiring Board with Electronic Components," Journal of IES, 1991, pp. 25-31.
- [27]. Jih, E.; and Jung, W.; "Vibration Fatigue of Surface Mount Solder Joints," Proceedings of Inter Society Conference on Thermal Phenomena, 1998, pp. 246-250.
- [28]. Wong, T.E.; Reed, B.A.; Cohen, H.M.; and Chu, D.W.; "Development of BGA Solder joint Vibration Fatigue Life Prediction Model," 49th Electronic Components & Technology Conference, San Diego, CA, 1999, pp. 149-154.
- [29]. Li, R.S.; "A Methodology for Fatigue Prediction of Electronic Components under Random Vibration Load," Transactions of the ASME, Vol. 123, 2001.
- [30]. Perkins, S.; "Vibration-Induced Solder Joint Fatigue Failure of a Ceramic Column Grid Array (CCGA) Package," 2004 Electronic Components and Technology Conference Proceedings, Las Vegas, 2004.
- [31]. Ramakrishnan, A.; and Pecht, M.; "Life Consumption Monitoring Methodology for Electronic Systems," IEEE Transactions on Components and Packaging technologies, Vol. 26, No. 3, September 2003, pp. 625-634.
- [32]. Mishra, S.; Pecht, M.; Smith, T.; McNee, I.; and Harris, R., "Remaining Life Prediction of Electronic Products Using Life Consumption Monitoring Approach," Proceedings of the European Microelectronics Packaging and Interconnection Symposium, Cracow, June 16-18, 2002, pp. 136-142.
- [33]. Shetty, V.; Das, D.; Pecht, M.; Hiemstra, D.; and Martin, S.; "Remaining Life Assessment of Shuttle Remote Manipulator System End Effector," Proceedings of the 22nd Space Simulation Conference, Ellicott City, MD, October 21-23, 2002.
- [34]. Mathew, S.; Das, D.; Osterman, M.; Pecht, M.; and Ferebee, R.; "Prognostic Assessment of Aluminum Support Structure on a Printed Circuit Board," International Journal of Performability Engineering, Vol. 2, No. 4, October, 2006, pp. 383-395.

- [35]. Mathew, S.; Das, D.; Osterman, M.; Pecht, M.; Ferebee, R.; and Clayton, J.; "Virtual Remaining Life Assessment of Electronic Hardware Subjected to Shock and Random Vibration Life Cycle Loads," *Journal of the IEST*, Vol. 50, No. 1, April 2007, pp 86-97.
- [36]. Simons, J.W.; and Shockey, D.A.; "Prognostics Modeling of Solder Joints in Electronic Components," *Aerospace Conference*, IEEE, March 2006.
- [37]. Nasser, L.; and Curtin, M.; "Electronics Reliability Prognosis Through Material Modeling and Simulation," *IEEE Aerospace Conference*, Big Sky, March 2006.
- [38]. Searls, D.; Dishongh, T., and Dujari, P.; "A Strategy for Enabling Data Driven Product Decisions through a Comprehensive Understanding of the Usage Environment," *Proceedings of IPACK'01 Conference*, Kauai, Hawaii, USA, July 8–13, 2001. pp. 1279–1284.
- [39]. Herbst, G.; "IBM's Drive Temperature Indicator Processor (Drive-TIP) Helps Ensure High Drive Reliability," *IBM White Paper*, <http://www.hc.kz/pdf/drivetemp.pdf>, viewed in September 2005.
- [40]. Vichare, N.; Rodgers, P.; Eveloy, V.; and Pecht, M.; "In-Situ Temperature Measurement of a Notebook Computer - A Case Study in Health and Usage Monitoring of Electronics," *IEEE Transactions on Device and Materials Reliability*, Vol. 4, No. 4, December 2004, pp. 658-663.
- [41]. Vichare, N.; Rodger, P.; Eveloy, V.; and Pecht, M.; "Environment and Usage Monitoring of Electronic Products for Health Assessment and Product Design," *International Journal of Quality Technology and Quantitative Management*, 2006.
- [42]. Bodenhofer, K.; "Environmental Life Cycle Information Management and Acquisition – First Experiences and Results from Field Trials," *Proceedings of Electronics Goes Green 2004+*, Berlin, September 5-8, 2004, pp. 541-546.
- [43]. ELIMA Report; "D-19 Final Report on ELIMA Prospects and Wider Potential for Exploitation," April 30, 2005, www.ELIMA.org, last accessed on December 2005.
- [44]. Tuchband, B.; and Pecht, M.; "The Use of Prognostics in Military Electronic Systems," *Proceedings of the 32nd GOMACTech Conference*, Lake Buena Vista, FL, March 19-22, 2007, pp. 157-160.
- [45]. Vichare, N.; and Pecht, M.; "Prognostics and Health Management of Electronics," *IEEE Transactions on Components and Packaging Technologies*, Vol. 29, No. 1, March 2006, pp. 222-229.

- [46]. Mishra, S.; and Pecht, M.; "In-situ Sensors for Product Reliability Monitoring," Proceedings of SPIE, Vol. 4755, 2002, pp. 10-19.
- [47]. Ridgetop Semiconductor-Sentinel Silicon TM Library, "Hot Carrier (HC) Prognostic Cell," August 2004.
- [48]. Anderson, N.; and Wilcoxon, R.; "Framework for Prognostics of Electronic Systems," Proceedings of International Military and Aerospace/Avionics COTS Conference, Seattle, WA, August 3-5, 2004.
- [49]. Goodman, D.; Vermeire, B.; Ralston-Good, J.; and Graves R.; "A Board-Level Prognostic Monitor for MOSFET TDDB," IEEE Aerospace Conference, Big Sky, 2006.
- [50]. Lall, P.; Hande, M.; Bhat, C.; Islam, N.; Suhling, J.; and Lee, J.; "Feature Extraction and Damage-precursors for Prognostication of Lead-free Electronics," 56th Electronic Components and Technology Conference, May, 2006.
- [51]. Harris, R.; and McNee, I.; "Physics of Failure (PoF) Approach to Life Consumption Monitoring (LCM) for Military Vehicles, Part 2," Third International Conference on Health and Usage Monitoring – HUMS 2003, pp. 55-64.
- [52]. Vichare, N.; Rodgers, P.; and Pecht, M.; "Methods for Binning and Density Estimation of Load Parameters for Prognostics and Health Management," International Journal of Performability Engineering, Vol. 2, No. 2, April 2006.
- [53]. Pecht, M.; Product Reliability, Maintainability, and Supportability Handbook, CRC Press, New York, 1995.
- [54]. Vichare, N.; Rodgers, P.; Eveloy, V.; and Pecht, M.; "Environment and Usage Monitoring of Electronic Products for Health (Reliability) Assessment and Product Design," IEEE Workshop on Accelerated Stress Testing and Reliability, Austin, Texas, Oct, 2005.
- [55]. Vichare, N.; "Prognostics and Health management of Electronics by Utilizing Environmental and Usage Loads," Ph.D. Dissertation, Dept. of Mechanical Engineering, University of Maryland, College Park, 2006.
- [56]. Wu, M.L.; "Rapid Assessment of BGA Fatigue Life under Vibration Loading," Ph.D. Dissertation, Dept. of Mechanical Engineering, University of Maryland, College Park, 2006.

- [57]. Engel, S.J., Gilmartin, B.J., Bongort, K., and Hess, A. 2000. Prognostics, The Real Issue Involved with Predicting Life Remaining. IEEE Aerospace Conference Proceedings, Big Sky, MT, USA, pp. 457-469.
- [58]. Lindman, H. R.; Analysis of Variance in Complex Experimental Designs, W.H. Freeman & Co, San Francisco, 1974.
- [59]. Vichare, N.; and Pecht, M.; “Enabling Electronic Prognostics Using Thermal Data,” Proceedings of the 12th International Workshop on Thermal Investigation of ICs and Systems, France, 2006, pp. 27-29.
- [60]. Chen, Y.; “Predicting the Vibration Fatigue Lives of Electronic Components Mounted on a PWB,” Ph.D. Dissertation, Dept. of Mechanical Engineering, University of Maryland, College Park, 1993.
- [61]. Kotlowitz, R.W.; and Taylor, L.R.; “Compliance Metrics For the Inclined Gull-wing, Spider J-bend, and Spider Gull-wing Lead Designs For Surface Mount Components,” IEEE Transactions on Components, Hybrids, and Manufacturing Technology, Volume 14, Issue 4, Dec. 1991 pp: 771 – 779.
- [62]. Gu, J.; Vichare, N.; Tinsley E.; and Pecht, M.; “Notebook Usage Monitoring for Design and Reliability Test,” accepted by IEEE Transactions on Components and Packaging Technologies.
- [63]. Dieter, G.E.; Mechanical Metallurgy, McGraw-Hill Book Co, 1988.
- [64]. IPC-SM-785, “Guidelines for Accelerated Reliability Testing of Surface Mount Solder Attachments”, 1992.
- [65]. Vishay quality control of strain gage installations, http://www.vishay.com/brands/measurements_group/guide/ta/qc/qc.htm, last accessed on 02/07/2007.
- [66]. Vishay technique note TN-507-1, http://www.intertechnology.com/Vishay/pdfs/TechNotes_TechTips/TN-507.pdf, last accessed on 02/07/2007.
- [67]. Vishay technique note TN-511, http://www.intertechnology.com/Vishay/pdfs/TechNotes_TechTips/TN-511.pdf, last accessed on 02/07/2007.
- [68]. Vishay technique note TN-505-4, http://www.intertechnology.com/Vishay/pdfs/TechNotes_TechTips/TN-505.pdf, last accessed on 02/07/2007.

- [69]. Izenman, A.J.; “Recent Developments in Non Parametric Density Estimation,” Journal of American Statistical Association, Vol. 86, No. 413, 1991, pp. 205-213.
- [70]. CALCE project C05-04 report: “Experiments to validate calcePWA vibration damage model with PbSn and SAC305”.
- [71]. ReliaSoft’s Accelerated Testing Reference
- [72]. Minitab 14 Tutorials
- [73]. Sobczyk, K.; and Spencer, B.F.; Random Fatigue: From Data to Theory. Academic Press, Inc. 1992.
- [74]. Intel Packaging Databook, <http://www.intel.com/design/packtech/packbook.htm>, last accessed on 02/09/2007.
- [75]. PCB standard capability, http://www.ccza.com/standard_capabilities.htm, last accessed on 02/07/2007.
- [76]. PCB roadmap, <http://www.ttmtech.com/technology/roadmap.htm>, last accessed on 02/07/2007.
- [77]. Circuit manufacturing minimums and tolerances, <http://www.tech-etch.com/flex/capabilities.html>, last accessed on 02/07/2007.
- [78]. Practical Components Catalog. 2004. <http://www.practicalcomponents.com/pdf/practcat.pdf>, last accessed on 11/03/2006.
- [79]. Ayyub, B.M.; and Klir, G.J.; Uncertainty Modeling and Analysis in Engineering and the Sciences, Chapman and Hall/CRC, 2006.
- [80]. Collins, J.; Failure of Materials in Mechanical Design, John Wiley & Sons, New York, NY, 1993.
- [81]. Mishra, S.; “Life Consumption Monitoring for Electronics,” Master Dissertation, Dept. of Mechanical Engineering, University of Maryland, College Park, 2003.